JOURNAL OF PETROLOGY

Journal of Petrology, 2015, Vol. 56, No. 11, 2089–2116
doi: 10.1093/petrology/egv064
Original Article

OXFORD

Magmas Erupted during the Main Pulse of Siberian Traps Volcanism were Volatile-poor

Svetlana Sibik[1]*, Marie Edmonds[1], John Maclennan[1] and Henrik Svensen[2]

[1]Department of Earth Sciences, University of Cambridge, Downing Street, Cambridge CB2 3EQ, UK and [2]Centre for Earth Evolution and Dynamics, University of Oslo, PO Box 1027 Blindern, 0316 Oslo, Norway

*Corresponding author. E-mail: spn31@cam.ac.uk

Received February 11, 2015; Accepted October 19, 2015

ABSTRACT

The eruption of the Siberian Traps Large Igneous Province (SLIP) at the Permo-Triassic boundary was synchronous with environmental degradation and the largest known mass extinction in the geological record. The volatile emissions associated with these eruptions have been linked to the environmental change yet we understand little of their source and magnitude and how they varied with time. There are a number of possible sources for the volatiles that were emitted during the eruptions: the mantle (including metasomatized lithosphere), volatile-rich sediments (through metamorphism or direct assimilation) and the crustal basement. To assess the relative importance of these sources (with the exception of the metamorphic outgassing source), we have conducted a geochemical study of melt inclusions hosted by clinopyroxene in Siberian Traps low-Ti tholeiitic lavas and sills of the Khakanchansky, Ayansky and Khonnamakitsky Formations. The magmas were not emplaced into or erupted onto evaporite deposits, in contrast to samples studied previously. The trace element compositions of the melt inclusions are highly variable compared with the uniform whole-rocks, exhibiting a wide range of La/Yb ratios from 0·7 to 9·5. The melt geochemistry is consistent with relatively large degrees of partial melting of a dominantly peridotite mantle source. A negative Nb anomaly indicates a degree of crustal contamination, but there is no evidence for contamination by volatile-rich evaporites. Enrichment of some of the melts in large ion lithophile elements (Ba, Sr) indicates their interaction with a fluid. We suggest that, consistent with the observed depletion in other incompatible trace elements in the melt inclusions, the volatile concentrations in the melts were relatively low, and that subsequently the melts underwent variable degrees of degassing in the crust. Overall, the melts are more volatile-poor than those reported previously from the SLIP and were erupted after the first "pulse" of more volatile-rich magmas described by Sobolev *et al.* (2015). These volatile-poor magmas may have been widespread across the region during the Siberian Traps eruptions once a pyroxenite component in the mantle source had been exhausted.

Key words: melt inclusions; Siberian Traps; trace elements; volatiles; degassing

INTRODUCTION

The eruption of the Siberian Traps Large Igneous Province (SLIP) (Fig. 1) took place at the Permo-Triassic boundary and was synchronous with the largest known mass extinction (Erwin, 1990; Renne & Basu, 1991; Kamo *et al.*, 2003; White & Saunders, 2005; Reichow *et al.*, 2009; Burgess *et al.*, 2014). It is likely that the enormous quantities of volatiles outgassed to the atmosphere during the prolonged volcanism were an important causal factor in severe environmental degradation, which may have led to climate change and ocean anoxia (Campbell *et al.*, 1992; Renne *et al.*, 1995; Wignall, 2001), although the processes and feedbacks are likely to have been complex (Self *et al.*, 2005; Mather, 2008). To understand this link, records of the volatile budget of the magmas involved in the Siberian

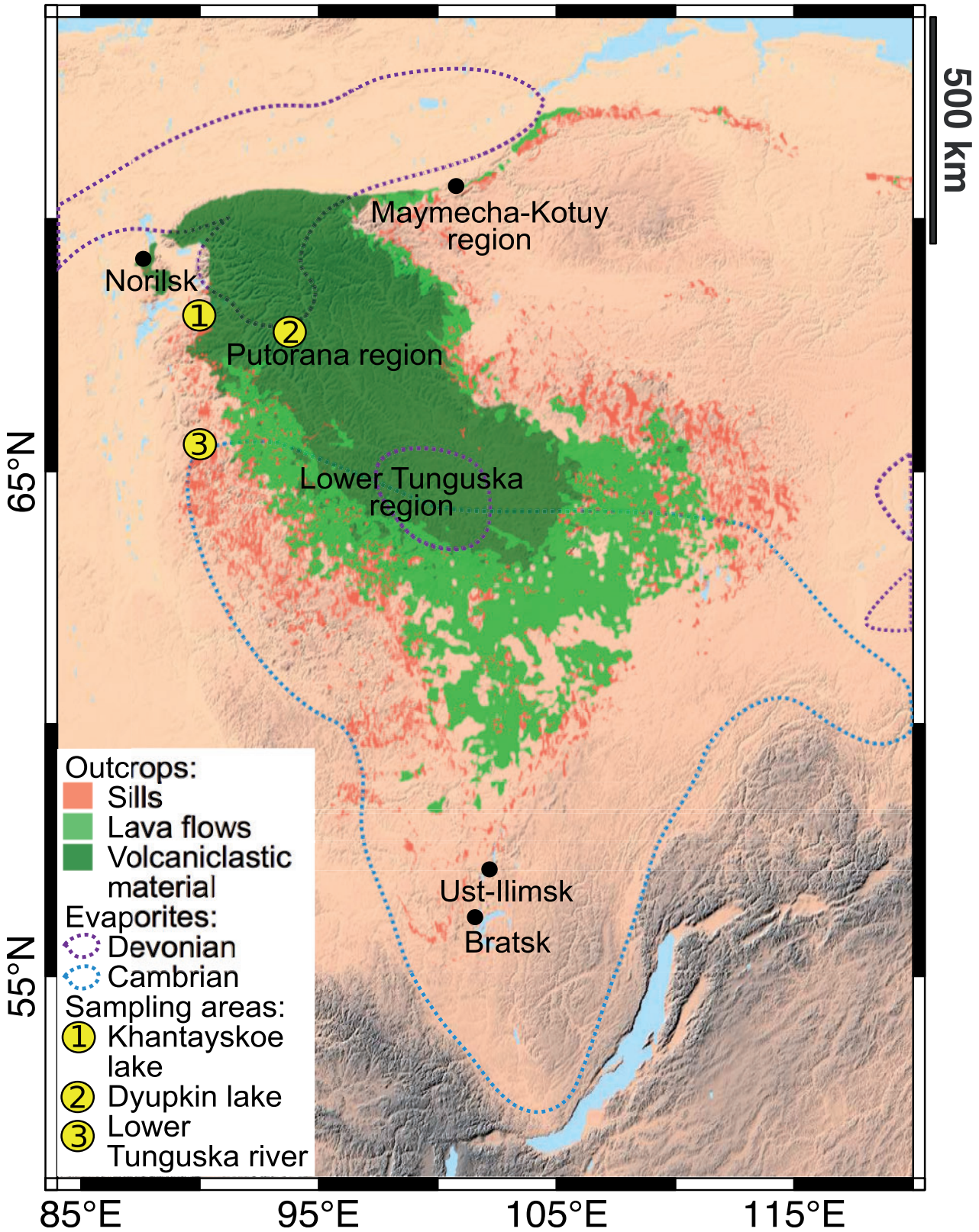

Fig. 1. Schematic geological map of the Siberian Craton and the Tunguska Basin, showing the distribution of outcrops of sills, lava flows and volcaniclastic deposits [modified from Malich *et al.* (1974)]. The distribution of Devonian and Cambrian evaporites is from Zharkov (1984) and Petrychenko *et al.* (2005). Sampling areas indicate the locations of samples from which melt inclusions were analysed.

Traps volcanism must be sought and the sources and magnitudes of the fluxes of volatiles estimated (e.g. Self *et al.*, 2005; Svensen *et al.*, 2009; Black *et al.*, 2012; Iacono-Marziano *et al.*, 2012; Tang *et al.*, 2013).

Siberian Traps lavas crop out on the Siberian Craton and form a discontinuous subcrop in the West Siberian Basin (Zolotukhin & Al'Mukhamedov, 1988; Reichow *et al.*, 2002, 2005). Estimates of the total maximum area of the magmatic province range from 4·3 million km^2 (Vasiliev *et al.*, 2000) to 5 million km^2 (Reichow *et al.*, 2009), which makes the SLIP the largest amongst all continental flood basalt provinces. The prevailing hypothesis for the origin of the SLIP involves the impact of a mantle plume with temperatures up to 1500–1580°C at the base of 130–180 km thick lithosphere (Richards *et al.*, 1989; Renne & Basu, 1991; Basu *et al.*, 1995; Sobolev *et al.*, 2009). The lack of expected uplift that the upwelling of hot asthenosphere should produce has been explained by: edge-driven convection accompanied by lithospheric melting and delamination (Anderson, 1994; Czamanske *et al.*, 1998; Elkins-Tanton & Hager, 2000); the presence of ~15% recycled oceanic crust in the head of a superplume, which would have led to only minor regional uplift owing to the presence of high-density eclogite (Sobolev *et al.*, 2009); or flux melting owing to the dehydration of a cold, stagnant subducted slab (Ivanov & Litasov, 2014). Alternatively, Saunders *et al.* (2005) proposed that the uplift occurred in the West Siberian Basin and the evidence for it was buried beneath a thick sediment pile.

It has been shown that the total volatile budget of the SLIP was complex: volatiles were probably sourced from the mantle itself (Sobolev *et al.*, 2009, 2011) and from the crust, including from volatile-rich sediments (Svensen *et al.*, 2009). Sourcing volatiles from the crust requires either bulk assimilation and melting of the assimilated material (Black *et al.*, 2012) or outgassing of the country rocks through contact metamorphism (Svensen *et al.*, 2009; Aarnes *et al.*, 2010, 2011). In the former scenario, the geochemical signature of the assimilation would be preserved in both erupted magmas and sills. The analysis of whole-rock basalts (Grinenko, 1985; Ripley *et al.*, 2003) and melt inclusions (Black *et al.*, 2014) shows that sulfur isotope compositions are enriched to different extents in ^{34}S over ^{32}S, which might be explained by the assimilation of isotopically heavy anhydrite-dominated evaporite deposits (Black *et al.*, 2014), which are prevalent in much of the region (Fig. 1). Extensive outgassing owing to contact metamorphism is believed to have significantly augmented the total Siberian Traps volatile budget (Svensen *et al.*, 2009). This process is unlikely to have preserved any geochemical signature in the magmas, although the flow of metamorphic fluids into sills has been proposed for intrusions at Duluth, Minnesota, on the basis of osmium isotopic variations (Ripley *et al.*, 2001). The sediment devolatilization mechanism could also explain the extreme negative excursions in the carbon isotope record in contemporaneous sediments (Baud *et al.*, 1989) by means of outgassing of isotopically light methane derived from metamorphism (Ganino & Arndt, 2009; Svensen *et al.*, 2009). Such excursions may also be attributed to decreased light carbon removal as a consequence of less active productivity of marine species (Brasier *et al.*, 1996; Kaufman *et al.*, 1996; Isozaki, 1997; White, 2002).

Previous studies of Siberian Traps magmatic rocks have demonstrated enormous geochemical diversity (Lightfoot *et al.*, 1990, 1993; Wooden *et al.*, 1993; Hawkesworth *et al.*, 1995). The early high-Ti basaltic series of the SLIP (Ivakinsky, Syveminsky, Gudchikhinsky; Fig. 2) are thought to have formed from melting of a pyroxenite mantle source and represent the first pulse of the eruption (Sobolev *et al.*, 2011); low-Ti magmas (e.g. Tulkonsky, Mokulaevsky, Samoedsky Formations; Fig. 2), sourced from a peridotite mantle, erupted later (Fedorenko *et al.*, 1996). The most primitive melt compositions found, as inclusions hosted in $Fo_{79·1–82·8}$

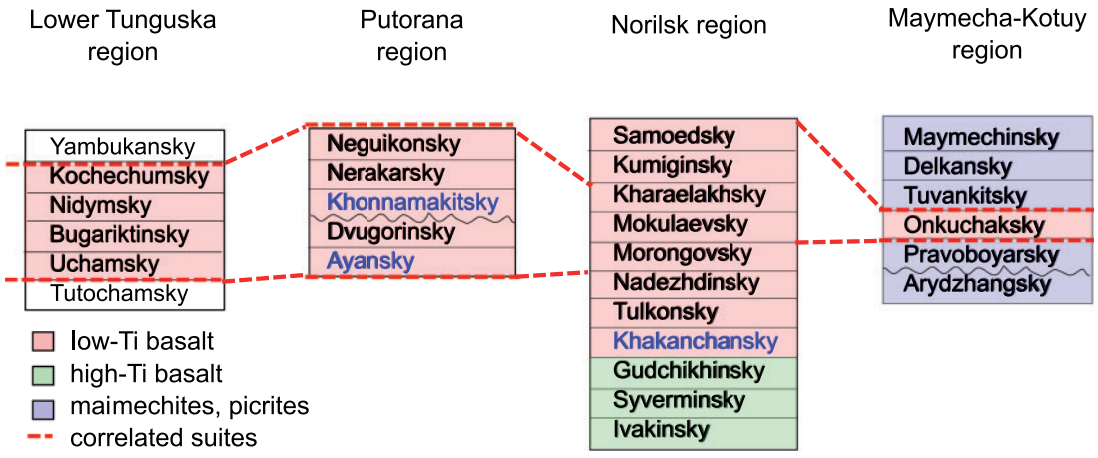

Fig. 2. Schematic stratigraphy of the Lower Tunguska, Putorana, Norilsk and Maymecha–Kotuy regions of the Siberian Traps (see Fig. 1 for locations). Modified from the Soviet regional stratigraphic scheme for Triassic deposits of the Tungusskaya syncline and Kuznetsk Basin. Melt inclusions were analysed in samples from formations whose names are highlighted in blue.

olivines from the Gudchikhinsky Formation (Fig. 2), are thought to be derived from melting of a pyroxenite mantle source and are not contaminated by continental crust, in contrast to the lavas of the Ivakinsky and Syverminsky Formations, which show evidence for contamination by continental crust (see below; Wooden *et al.*, 1993; Sobolev *et al.*, 2009, 2011). Low-Ti Siberian Traps magmas form the main magmatic series and make up the largest volume of emplaced sills and lavas (Wooden *et al.*, 1993; Reichow *et al.*, 2005). They have undergone variable degrees of crustal contamination, varying from high (Nadezhdinsky Formation) to insignificant (e.g. Mokulaevsky and Kumingsky Formations) (Fig. 2).

The primary melt reconstructed from melt inclusions from the Gudchikinhsky Formation (Fig. 2) is poor in sulfur (400 ± 200 ppm) but rich in chlorine (~350–400 ppm) compared with typical mantle-derived primary melts (Sobolev *et al.*, 2009). It has been proposed that these melts were derived from a mantle source containing a significant proportion of chlorine- and carbon-rich recycled oceanic crust (i.e. pyroxenite). The degassing and eruption of such melts would have caused substantial HCl and CO_2 outgassing prior to the main magmatic pulse, thereby perhaps triggering the mass extinction (Sobolev *et al.*, 2011). The hypothesis, initially proposed by Hofmann & White (1982), that the pyroxenite component of a heterogeneous mantle source melts out first, generating a change in the character of melts with time, is not unique to the SLIP. Recent studies have demonstrated that a certain proportion of enriched recycled oceanic crust, variably enriched in volatiles, could be present in the mantle source regions of the Karoo Province (Heinonen *et al.*, 2014), Cook Islands (Cabral *et al.*, 2013), Hawaii (Sobolev *et al.*, 2005) and Iceland (Shorttle & Maclennan, 2011).

Melt inclusions in olivines in both ore-bearing (Talnakh) and barren (Zelenaya Griva and Nizhniy Talnakh) intrusions in the Norilsk region are rich in chlorine (from 0·01 to 0·61 wt %) and sulfur (from 0·01 to 0·14 wt %) (Krivolutskaya, 2001). High halogen contents are also observed in melt inclusions in basalts from south and NE of the Siberian Craton: plagioclase- and olivine-hosted melt inclusions from the Ust-Ilimsk and Bratsk dolerite sills (Fig. 1) have chlorine contents of 0·01–0·78 wt %, sulfur contents of 0·01–0·17 wt % and fluorine contents of 0·02–1·95 wt % (Black *et al.*, 2012). Such high volatile contents have been linked to the assimilation of Cambrian evaporites, which are predominant in the south of the platform, into which the magmas were intruded (Black *et al.*, 2012). The origin of high fluorine concentrations in those melt inclusions is inconsistent with salt assimilation as seawater does not contain sufficient fluorine. Fluorine may have come from sulfate evaporites, sedimentary phosphorite deposits or fluorite mineralization, which is found locally on the Craton. Variable assimilation of evaporites is supported by a range in Cl/K ratios at a constant K_2O content of the melt inclusions and by the circumstantial evidence of thick salt layers in the south of Tunguska Basin, from which these samples originated (Black *et al.*, 2012). Volatile abundances are similarly high in melt inclusions in meimechites located in the NE of the region (Fig. 1; Black *et al.*, 2012). These highly magnesian alkaline rocks are thought to have formed at the lowest degrees of harzburgite melting at a depth of >200 km (Arndt *et al.*, 1995, 1998). Melt inclusions in olivines from these rocks contain 0·02–0·51 wt % S, 0·01–0·15 wt % Cl and 0·02–0·16 wt % F on average (Black *et al.*, 2012). Low degrees of peridotite or harzburgite melting at high pressures of 6–8 GPa (Arndt *et al.*, 1998) and delaminated lithosphere mixed with metasomatized harzburgite (Sobolev *et al.*, 2009) have been proposed to contribute to the volatile budget of the meimechite melts. Overall, however, these extremely volatile-rich magmas (meimechites and sills intruded into Cambrian evaporites), constitute less (perhaps much less) than 10% of the total magma volume of the SLIP (Vasiliev *et al.*, 2000) and are not representive of the vast volumes of tholeiitic Siberian magmas.

In this study we report whole-rock and melt inclusion compositional data for the Khakanchansky, Ayansky and Khonnamakitsky Formations erupted in the region SE of Norilsk (Figs 1 and 2). This represents the first melt inclusion study of the magmas from the low-Ti series. The lavas and sills sampled for this study were not directly emplaced into or erupted onto evaporite deposits (Fig. 1); however, we acknowledge that the magmas could have potentially encountered evaporites at depth. As a result, we would not expect evaporite assimilation to have played an important role in their petrogenesis. The magmatic rocks analysed here are representative of the vast volumes of tholeiitic lavas erupted as part of the main magmatic pulse, emplaced after the pyroxenite-derived melts analysed by Sobolev *et al.* (2009). A major aim of this work is to assess whether these magmas were as volatile-rich as the melts inferred to be derived from a mantle source containing recycled oceanic crust that erupted earlier in the SLIP sequence (Sobolev *et al.*, 2009) or whether they have a more depleted signature, consistent with large degrees of melting of peridotite. We use the trace element and volatile geochemistry of the melt inclusions to deconvolve mantle-derived, primary melt compositions and heterogeneity from the effects of crustal contamination, fluid signatures and degassing. Understanding the role of heterogeneous mantle plumes in supplying volatiles to the atmosphere and the time-evolution of large and sustained periods of volcanism is of great importance for explaining the contemporaneous environmental degradation.

SAMPLING AND METHODS

Sampling area

For this study, we use samples of sills and lava flows from Khantayskoe lake, Dupkin lake, and the Kureika and Lower Tunguska river regions south of Norilsk

(Fig. 1). The samples were collected from surface outcrops (see Supplementary Data A1 for geographical coordinates) during a 2010 expedition led by the University of Oslo. The basalts and dolerites belong to the Khakanchansky, Ayansky and Khonnamakitsky Formations in the Norilsk and Putorana regions (Figs 1 and 2) (see also Supplementary Data A1 for more details about the samples; supplementary data are available for downloading at http://www.petrology.oxfordjournals.org). The crystals hosting the melt inclusions were picked from two lava flows (samples S10–3 and S10–19) and one sill (sample S10–44) from three locations (Khantayskoe lake, Dyupkin lake and the Lower Tunguska river).

Bulk-rock analysis

Nineteen samples were analysed for bulk-rock major and trace elements by inductively coupled plasma atomic emission spectrometry (ICP-AES) and inductively coupled plasma mass spectrometry (ICP-MS) at the University of London, Royal Holloway. Powders for geochemical analyses were prepared from about 10 g of fresh rock chips using a tungsten Tema mill; 0·2 g of powdered sample was weighed into a graphite crucible and 1·0 g of $LiBO_2$ was added. The powders were carefully mixed and fused at 900°C for 20 min, then dissolved in 200 ml of cold 5% nitric acid. Ga was added to the flux to act as an internal standard. This solution was then analysed for Si, Al and Zr by ICP-AES using a Perkin Elmer Optima 3300R system calibrated with natural and synthetic standards. The solution was also used to analyse for Cs, Nb, Rb, Ta, Th, Tl, U, Y, and rare earth elements (REE) by ICP-MS on a Perkin Elmer Elan 5000 system calibrated with natural and synthetic standards. Another batch of 0·2 g of powdered sample was dissolved in 6 ml of HF and $HClO_4$ (2:1 mixture), evaporated to dryness, cooled and dissolved in 20 ml of 10% HNO_3. This solution was analysed by ICP-AES for Fe, Mg, Ca, Na, K, Ti, P, Mn, Ba, Co, Cr, Cu, Li, Ni, Pb, Sc, Sr, V, and Zn. The details on accuracy and precision of the measurements are provided in Supplementary data A2.

Micro-analytical methods

Clinopyroxene and olivine grains were hand-picked from crushed and sieved whole-rock material in the size fraction 250–500 μm. All the melt inclusions in the selected clinopyroxenes and olivines were wholly crystalline. Rehomogenization was carried out in a 1 atm vertical gas-mixing furnace. Clinopyroxene and olivine grains were wrapped in a platinum foil envelope and suspended in the furnace with a platinum wire. In the furnace, the samples were heated to the target temperature (1190–1200°C), held there for 20 min and then quenched rapidly in water. The oxygen fugacity was maintained at FMQ – 1 (where FMQ is fayalite–magnetite–quartz) with a mixture of CO and CO_2 gases. The grains did not oxidize and crystalline melt inclusions became fully homogeneous and crystal-free, although in some melt inclusions a bubble remained after rehomogenization (Fig. 3b). Single grains were mounted in stubs with epoxy resin and polished to expose the melt inclusions.

To acquire a complete geochemical analysis, including volatile, major and trace elements for the same melt inclusions, which were largely 10–20 μm in diameter, trace elements and volatiles were measured first by secondary ion mass spectrometry (SIMS) using an oxygen beam, followed by electron probe microanalysis (EPMA) for major elements and chlorine. Microanalysis of 43 rehomogenized melt inclusions hosted by clinopyroxene was carried out.

Melt inclusions were analysed for sulfur, fluorine and carbon dioxide, on a Cameca IMS-1270 system, followed by trace element analysis on a Cameca IMS-4f system at the University of Edinburgh. The stubs with mounted grains were gold-coated to remove the extra surface charge and loaded into the chamber 24 h in advance to outgas and create sufficient vacuum. For the measurements of volatile elements melt inclusions were bombarded with a 15–20 μm diameter beam of oxygen O_2^- with 12·2 kV primary voltage and 3·3 nA current. To remove any surface contamination the beam was rastered over the surface for 60 s with a 10 μm raster and only the last 10 cycles out of the 20 measured were used. The same pits in the melt inclusions were then used for the analysis of trace elements. Negative oxygen O^- was used as a primary ion beam of 10·8 kV and a beam current of 6·6 nA. The secondary ions were accelerated at a voltage of 4·5 kV minus a 75 eV offset. The calibration of volatiles was performed using the standards VG-2, VG-A99, NIST-610 and BCR-2G reported by GeoRem (http://georem.mpch-mainz.gwdg.de). The detection limits for carbon dioxide, fluorine and sulfur were less than 10 ppm. Thus, the errors for sulfur and fluorine averaged 2·41% and 9·59%, respectively, for glasses with less than 200 ppm of each volatile (see Supplementary Data A3 for calibration details, accuracy and precision of S, F and CO_2 measurements). The analyses of standards indicated different accuracies for the trace elements varying from 15·4% for Ba to 0·75% for Yb (Supplementary Data A4). The analytical precision is better than 3% for all trace elements except Sm, Dy, and Tm, for which it is up to 4·8% based on repeat measurements.

Major element compositions of host clinopyroxenes and melt inclusions were determined by electron microprobe (Cameca SX100) at the University of Cambridge. Glass analyses were performed with a spot size of 5 μm, an operating potential of 15 kV and a beam current of 10 nA. Mineral analyses were performed with an operating potential of 15 kV, beam current of 20 nA and a beam size of 1 μm. Counting times for clinopyroxene analyses for different elements were 10 s for Na and K, 20 s for Fe and Si, 30 s for Mg, Al, Cr and Mn, 60 s for Ni and Ca, and up to 120 s for Ti. Melt inclusions were analysed for a longer time: 150 s for Mg and Al, 60 s for Ti and Ca, 120 s for Fe, 90 s for Cr and Ni, 30 s for P and Mn, 20 s

for Si, 10 s for Na and K, and up to 260 s for Cl. Calibration standards were as follows: jadeite for Na, periclase for Mg, Si glass for Si, K-feldspar for K, rutile for Ti, fayalite for Fe, corundum for Al, apatite for P, pure metals for Cr, Mn and Ni, and halite for Cl. Data reduction was performed using the inbuilt Cameca X-Phi PeakSight software for glass analyses and PAP corrections for mineral analyses. Analyses with totals outside the range 98·5–100·5 wt % were discarded. For major elements the error of the measurement did not exceed 5%. For chlorine the detection limit was 150 ppm and the precision was 8·55%.

Post-entrapment modification of melt inclusion geochemistry

Rehomogenization in a furnace allows analysis of glassy melt inclusions for major and trace elements, as well as for volatiles. We neglect the effect of post-entrapment crystallization (PEC) and Fe loss (Danyushevsky *et al.*, 2000, 2002) that affects only melt crystallization on the inclusion rims. The possible congruent melting of the host mineral owing to overheating during homogenization of the melt inclusions in the furnace may lower the concentrations of some elements. This factor, if taken into account, would result in lower absolute concentrations of volatile and trace elements, depending on the amount of host mineral added to the melt. A second process will have an identical consequence: owing to the size of the inclusions (10–20 μm) being similar to the beam size, overlapping of the beam onto the host mineral during SIMS microanalysis should be considered. The effect of clinopyroxene host dilution (during reheating) or beam overlap is greater for those elements that are highly incompatible in clinopyroxene [e.g. light rare earth elements (LREE), Ba, Nb]; the decrease in content of these elements is proportional to the dilution factor. For those elements with high clinopyroxene–melt partition coefficients [e.g. heavy rare earth elements (HREE)], the dilution effect is less significant, especially for melt inclusions with lower enrichment in trace elements (Supplementary Data A5). The absolute difference in concentrations is more significant for highly enriched melts (e.g. S10–3 mi6). Thus, if 30%, which is considered to be a maximum probable proportion, of host clinopyroxene is overlapped or diluted into the inclusion, the relative decrease in concentrations of LREE is about 24–29·5%, whereas for HREE it ranges from 3 to 20% for depleted and enriched melt inclusions, respectively. The changes in trace element ratios are less significant: La/Yb is 13–16%, La/Sm 8–15% and Gd/Yb is 1–2% lower for highly and moderately enriched melt inclusions and 8% higher for depleted melt inclusions. Such variations owing to overlapping or dilution of the host clinopyroxene are substantially lower than the variability observed in the analysed melt inclusions. If the actual analyses demonstrate overlapped or diluted inclusions, then the true melt compositions would have been even more enriched in highly incompatible trace elements. Moreover, rehomogenization experiments did not influence the geochemistry of the inclusions beyond a thin boundary layer at the edges, according to the profiles through the melt inclusion (Supplementary Data A6).

During rehomogenization of the melt inclusions at liquidus temperatures, loss of volatiles by diffusion through the host crystal may occur. Although research has been carried on the diffusion rates of volatiles in silicate melts (Baker *et al.*, 2005; Freda *et al.*, 2005; Baker & Balcone-Boissard, 2009; Balcone-Boissard *et al.*, 2009), very few studies have investigated the diffusion of S, Cl and F in silicate minerals. It seems likely that fluorine, similar to hydrogen, may diffuse from the melt through olivine (and probably also clinopyroxene), whereas chlorine does not (Portnyagin *et al.*, 2008; Gaetani *et al.*, 2012; Le Voyer *et al.*, 2014). Although the diffusivity of sulfur in silicate melts is intermediate between that of chlorine and fluorine (Baker *et al.*, 2005), it has a relatively large ionic radius and so we assume that sulfur will not diffuse through the host crystal to any large degree on rehomogenization timescales.

All of the melt inclusions were examined thoroughly for the presence of cracks and fractures running through them. Despite inclusions affected by cracks being excluded from the reported dataset, the possibility of breaching cannot be eliminated. Contraction of magma during cooling may result in microfractures inside the crystals at the margins of the inclusions (Tait, 1992; Kent, 2008). Such cracks could further serve as pathways for hydrothermal fluids inside the inclusion, which may then change the concentrations of mobile (i.e. Na, K) and large ion lithophile elements (LILE; i.e. Ba, Rb, Sr). If these breached inclusions are then subject to rehomogenization in a furnace, volatiles may be lost from the inclusion. Low volatile contents may be a sign of breaching, but they might also be explained by pre-entrapment melt degassing. Trace elements in breached inclusions might show elevated concentrations of LILE, whereas REE and high field strength elements (HFSE) would not be significantly affected. However, principal component analysis performed both including and excluding volatiles did not show a component driving LILE, K and Na up whilst driving volatiles down (See Supplementary Data). We, therefore, conclude that breaching is not significant in influencing the composition of the melt inclusions described here.

RESULTS

Petrographic description and bulk compositions

Whole-rock compositions correspond to tholeiitic to subalkaline low-titanium basalts (Table 1). The mineral assemblage of the lava flows includes 70% clinopyroxene microphenocrysts set in a groundmass consisting of 25% plagioclase and 5% accessory minerals, such as biotite and ilmenite. Laths of plagioclase ~0·06–0·3 mm long are partly enclosed in elongated clinopyroxene

Table 1: Major and trace element composition of basalt flows and intrusions

Formation:	Khakanchansky		Ayansky					Khonnamakitsky		
	Basalt flows		Basalt flows					Basalt flows	Sills	
Location*:	KL		DL					KR	SR	LTR
Sample:	S10–3	S10–11	S10–12	S10–13	S10–15	S10–19	S10–22	S10–25	S10–29	S10–42
SiO_2	48·70	49·10	49·09	49·79	49·19	49·43	48·02	47·66	46·38	48·01
TiO_2	1·05	1·13	1·12	1·06	1·04	1·03	1·02	1·19	1·44	1·50
Al_2O_3	14·54	15·25	15·28	15·43	15·44	14·96	14·30	14·72	14·02	14·57
FeO_{tot}	11·54	12·44	12·65	12·34	12·18	11·99	11·56	12·93	13·63	13·95
MnO	0·17	0·20	0·19	0·19	0·19	0·17	0·17	0·20	0·20	0·21
MgO	6·69	7·19	7·42	7·71	7·57	7·29	6·96	6·60	6·71	6·93
CaO	11·10	11·31	11·23	11·81	11·59	11·58	11·09	10·80	9·67	10·03
Na_2O	2·01	2·05	2·05	2·12	1·92	1·89	1·88	2·21	2·30	2·40
K_2O	0·32	0·18	0·22	0·36	0·14	0·21	0·30	0·24	0·49	0·53
P_2O_5	0·14	0·15	0·15	0·14	0·13	0·13	0·13	0·14	0·19	0·20
LOI	3·26	1·07	1·02	0·21	1·33	1·50	1·24	1·70	0·27	0·30
Total	99·51	100·08	100·42	101·19	100·72	100·18	96·68	98·38	95·32	98·64
Ba	189·68	101·97	113·88	120·15	116·91	129·88	154·27	121·99	134·30	140·87
Co	44·58	48·53	48·92	50·08	49·44	47·24	45·68	48·42	48·33	50·68
Cr	146·30	158·67	138·05	167·34	163·59	98·94	158·17	135·80	149·60	166·32
Cs	1·74	0·15	0·15		0·01	0·22	0·24	0·34	0·29	0·61
Cu	98·66	120·45	126·31	124·71	116·32	95·32	110·34	138·23	180·91	157·70
Ga	16·52	17·07	16·93	16·96	16·50	16·06	16·13	17·66	18·03	18·79
Hf	2·24	2·05	1·93	1·92	1·80	1·90	2·07	1·96	3·19	3·00
Mo	0·95	1·10	1·00	0·05	0·84	0·98	0·96	0·97	0·94	0·86
Nb	3·74	4·31	3·05	2·98	2·15	3·03	4·16	2·34	5·12	4·54
Ni	98·89	122·40	124·62	127·45	129·09	99·72	101·50	102·00	120·33	124·36
Pb	3·55	2·42	1·80	0·14	1·70	2·01	2·67	2·45	2·03	2·26
Rb	10·46	4·24	6·42	3·87	1·29	2·25	3·86	11·39	11·25	12·49
Sb	0·14	0·13	0·18	0·01	0·16	0·17	0·16	0·17	0·15	0·09
Sc	35·41	37·12	36·86	37·75	37·41	36·46	35·41	35·83	34·96	36·11
Sn	0·63	0·57	0·54	0·03	0·44	0·56	1·17	0·72	0·86	0·60
Sr	265·66	204·21	204·52	196·48	187·28	215·86	205·44	202·82	176·88	186·43
Th	1·55	1·11	1·05	1·00	0·89	1·25	1·48	0·78	1·21	1·08
U	0·60	0·49	0·48	0·45	0·41	0·51	0·54	0·34	0·53	0·52
V	246·86	269·34	290·25	278·37	265·08	247·54	253·59	270·25	316·77	329·78
Y	22·25	24·36	23·91	23·32	22·36	21·44	22·10	23·89	28·86	30·26
Zn	103·03	88·25	74·63	6·31	83·25	92·16	90·33	97·77	103·01	109·34
Zr	99·88	97·07	92·57	85·44	80·51	88·67	95·88	86·62	109·68	119·02
La	8·46	6·59	6·91	6·43	5·75	7·63	8·40	6·65	7·13	7·46
Ce	18·26	14·94	14·76	14·09	12·84	16·11	17·41	13·45	16·57	17·19
Pr	2·35	2·01	2·01	1·88	1·75	2·08	2·30	1·88	2·32	2·39
Nd	11·71	10·50	10·57	10·27	9·50	10·71	11·46	10·31	12·44	13·14
Sm	3·01	2·93	2·87	2·84	2·62	2·70	2·83	2·86	3·58	3·73
Eu	0·83	0·88	0·83	0·85	0·82	0·82	0·81	0·89	1·07	1·07
Gd	3·41	3·51	3·46	3·44	3·17	3·20	3·38	3·41	4·36	4·40
Tb	0·50	0·53	0·52	0·52	0·49	0·48	0·50	0·53	0·64	0·68
Dy	3·74	3·91	3·91	3·79	3·55	3·52	3·67	3·89	4·78	4·92
Ho	0·67	0·72	0·69	0·68	0·66	0·63	0·64	0·70	0·86	0·90
Er	2·21	2·38	2·37	2·33	2·19	2·11	2·22	2·34	2·87	3·03
Tm	0·26	0·31	0·30	0·30	0·27	0·26	0·28	0·30	0·36	0·37
Yb	2·05	2·27	2·26	2·25	2·16	2·03	2·15	2·25	2·71	2·81
Lu	0·27	0·30	0·28	0·28	0·28	0·24	0·27	0·28	0·34	0·36

*(KL) Khantayskoe Lake; (DL) Dyupkun Lage; (KR) Kureika River; (SR) Severnaya River; (LTR) Lower Tunguska River.

microphenocrysts, which are up to 0·6 mm long, defining a sub-ophitic texture (Fig. 3a). Sills, as distinct from lava flows, contain ~5% of euhedral olivine phenocrysts up to 0·4 mm long with a forsterite content ranging from 46·5 to 51·2 mol %. The anorthite content of the plagioclase ranges from 52·2 to 63·8 mol % in lava flow S10–3, from 54·73 to 74·17 in S10–19 and from 46·92 to 77·36 in sill S10–25. (Supplementary Data A7). The samples from the Khakanchansky, Ayansky and Khonnamakitsky Formations are characterized by an average TiO_2 content of 1·09 (1·05–1·13), 1·05 (1·02–1·12) and 1·28 (0·92–1·73) wt % respectively (Table 1). They belong to the low-titanium upper basaltic sequence (see stratigraphy in Fig. 2). Rare earth and trace element patterns of the analysed sills and lavas (Fig. 4) demonstrate the overall geochemical variation of the studied formations. The bulk-rocks have Mg-numbers of 53·4–55·9 (Fig. 5).

Most of the analysed sediments that are associated with the studied lavas and sills (Supplementary Data A7) have a geochemical composition between average continental crust (Rudnik & Gao, 2003) and extremely

Table 1: Continued

Formation:	Khonnamakitsky								
	Sills							Dykes	
Location:	LTR							LTR	
Sample:	S10–44	S10–46	S10–47	S10–48	S10–61	S10–62	S10–67	S10–77	S10–80
SiO_2	48·44	47·42	50·03	51·00	46·90	52·85	37·86	45·95	47·97
TiO_2	1·09	1·73	1·25	0·93	1·69	0·92	1·00	1·05	1·51
Al_2O_3	15·61	14·07	14·27	14·81	14·01	15·67	11·81	14·22	15·25
FeO_{tot}	12·37	14·76	9·92	10·50	14·77	10·51	10·28	11·65	13·87
MnO	0·19	0·22	0·19	0·17	0·23	0·16	0·15	0·22	0·22
MgO	7·92	6·17	6·95	6·72	6·06	6·83	5·77	7·40	6·84
CaO	10·63	9·91	12·86	10·37	9·84	11·06	8·21	7·84	10·37
Na_2O	2·13	2·38	2·26	2·35	2·26	2·28	1·76	4·00	2·30
K_2O	0·46	0·47	0·51	1·16	0·52	0·98	0·29	0·99	0·72
P_2O_5	0·14	0·22	0·14	0·12	0·22	0·12	0·11	0·14	0·19
LOI	1·12	0·82	0·37	0·75	0·86	0·85	0·58	5·82	0·36
Total	100·08	98·17	98·75	98·88	97·37	102·24	77·84	99·28	561·4
Ba	109·74	138·01	140·43	346·46	145·47	179·97	91·99	190·30	48·5
Co	51·20	46·77	35·51	39·39	46·66	40·32	38·86	45·13	158·6
Cr	148·46	128·92	685·08	68·23	128·81	70·54	179·09	182·74	1·3
Cs	0·73	0·92	0·36	1·70	1·54	1·79	0·09	17·54	172·8
Cu	126·72	208·45	104·76	11·27	203·84	21·73	121·24	116·86	19·4
Ga	17·44	19·56	17·39	16·34	19·42	17·12	13·78	15·39	2·7
Hf	1·49	4·27	2·14	2·52	2·97	2·54	1·54	1·70	1·04
Mo	0·60	1·17	0·43	0·64	1·12	0·97	0·70	0·61	3·5
Nb	1·99	7·45	2·86	5·25	4·70	5·29	1·42	1·82	116·6
Ni	144·59	90·81	75·38	14·12	94·74	15·99	115·76	108·90	9·33
Pb	1·91	2·53	4·92	89·28	3·94	1·66	1·44	1·28	12·6
Rb	10·02	12·39	13·32	34·00	14·08	32·80	6·72	25·55	0·16
Sb	0·07	0·17	0·05	0·07	0·18	0·15	0·12	0·14	36·67
Sc	33·74	38·12	54·27	31·16	37·35	31·24	29·72	35·64	0·69
Sn	0·32	1·04	0·66	0·41	1·06	0·36	0·58	0·35	583·02
Sr	210·72	185·24	206·03	264·72	189·41	253·47	137·97	212·53	0·46
Th	0·69	1·26	0·71	2·43	1·01	2·59	0·56	0·79	0·9
U	0·35	0·54	0·29	0·70	0·52	0·79	0·24	0·34	0·4
V	246·50	348·87	399·79	217·45	350·07	218·98	221·87	250·29	343·1
Y	22·53	35·07	24·75	20·04	33·69	20·96	19·85	22·22	29·4
Zn	97·85	123·92	94·10	92·87	129·70	45·85	89·85	77·47	163·50
Zr	72·36	134·88	85·03	102·55	127·15	110·07	68·14	80·41	110·7
La	5·73	8·52	5·62	12·03	8·33	13·60	4·21	5·75	7·1
Ce	12·97	18·86	13·20	24·56	18·26	26·18	9·67	12·85	15·5
Pr	1·82	2·69	1·84	3·04	2·53	3·20	1·41	1·75	2·2
Nd	9·81	14·66	10·55	14·12	14·36	14·99	7·94	9·61	12·4
Sm	2·76	4·10	3·06	3·09	4·04	3·30	2·29	2·65	3·5
Eu	0·85	1·24	0·95	0·85	1·19	0·88	0·71	0·82	1·1
Gd	3·34	5·20	3·72	3·44	4·92	3·66	2·84	3·21	4·3
Tb	0·50	0·79	0·56	0·48	0·76	0·49	0·45	0·48	0·7
Dy	3·70	5·78	4·16	3·29	5·59	3·47	3·29	3·62	4·9
Ho	0·67	1·08	0·74	0·59	1·01	0·62	0·59	0·65	0·9
Er	2·24	3·45	2·43	1·98	3·34	2·09	1·95	2·17	2·9
Tm	0·28	0·44	0·30	0·24	0·40	0·25	0·24	0·28	0·4
Yb	2·12	3·33	2·26	1·83	3·23	1·94	1·89	2·05	2·8
Lu	0·26	0·41	0·28	0·22	0·39	0·24	0·23	0·27	0·4

Oxides and total are in wt %; trace elements are in ppm. LOI, loss on ignition.

enriched Bolgokhtokhsky granodiorite (Hawkesworth *et al.*, 1995). This continental crust composition is used in the modelling described in the section below.

Melt inclusion compositions

The Mg# (Mg-number) values of the host clinopyroxenes [defined by the molar ratio 100MgO/(MgO + FeO), assuming all iron is ferrous] vary from 69·2 to 82·5, with an average of 78·7 (Table 2, Fig. 5). Magnesium numbers of clinopyroxene microphenocrysts are significantly higher than forsterite contents in olivines (Table 2, Supplementary Data A7), as such clinopyroxenes likely have trapped more primitive melts. Only a very few melt inclusions were found in olivines, which were serpentinized, therefore we further only report the analysis of clinopyroxene-hosted melt inclusions. The major and trace element compositions of the melt inclusions are reported in Table 3. The compositions of the melt inclusions as a function of their host clinopyroxene Mg# are shown in Fig. 6. More primitive clinopyroxenes, with the higher Mg#, have higher MgO and FeO contents (Fig. 6a and b), whereas TiO_2, K_2O and SiO_2, as well as incompatible trace element concentrations, increase with

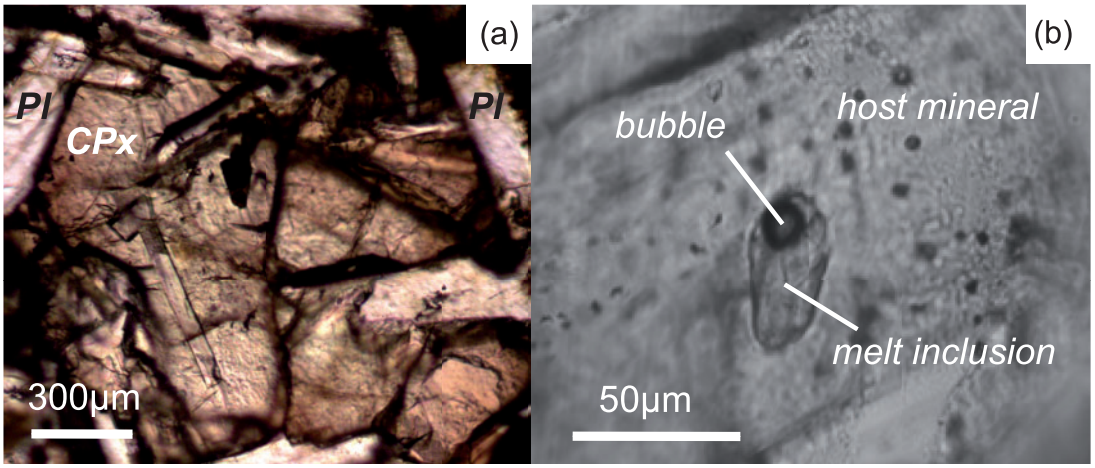

Fig. 3. (a) Lath-shaped plagioclase crystals enclosed within sub-ophitic titanaugite. (b) Clinopyroxene-hosted rehomogenized melt inclusion with a bubble.

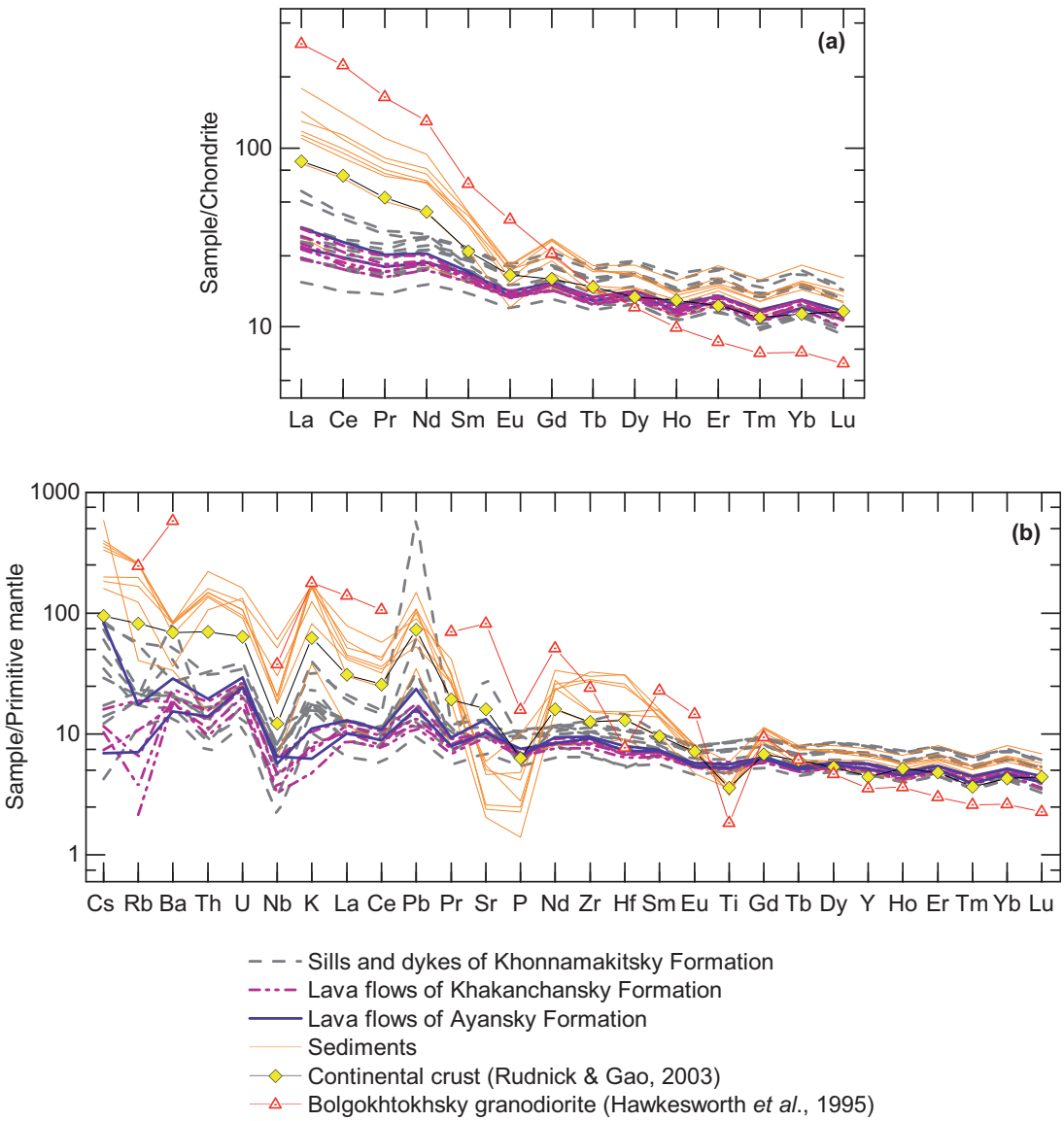

Fig. 4. (a) Rare earth and (b) multi-element patterns for analysed sills, dykes and lava flows, average continental crust (Rudnick & Gao, 2003), Bolgokhtokhsky granodiorite (Hawkesworth *et al.*, 1995) and local sediments. Concentrations are normalized to C1-chondrite values (Sun & McDonough, 1989) and Primitive Mantle values (McDonough & Sun, 1995), respectively.

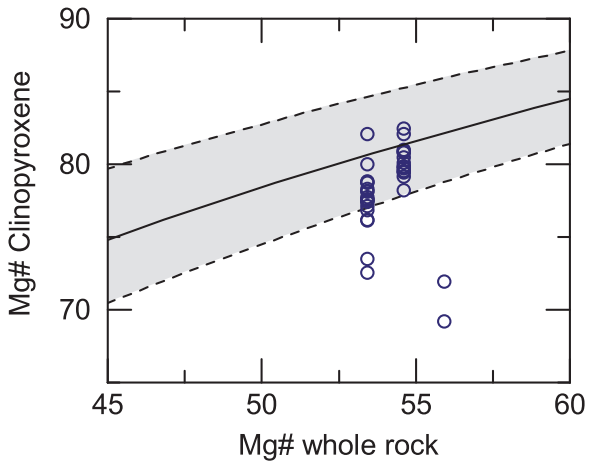

Fig. 5. Clinopyroxene compositions (Mg#) compared with the whole-rock Mg#, calculated with FeO set to 90% of the total iron in the whole-rock. The grey band shows the range of equilibrium clinopyroxene compositions for a given Mg-number (Mg#) when $K_D = 0{\cdot}275 \pm 0{\cdot}067$ (Putirka *et al.* 2003). The 2σ errors are smaller than the symbol size.

decreasing host crystal Mg# (Fig. 6d–i). Volatile contents (Fig. 6j–l) are independent of clinopyroxene Mg#.

REE and trace element profiles for both whole-rocks and melt inclusions are shown in Fig. 7, normalized with respect to chondritic abundances (Sun & McDonough, 1989). The compositions of local granodiorite (from Hawkesworth *et al.*, 1995), average continental crust (from Rudnick & Gao, 2003), the clinopyroxene hosts and "primitive uncontaminated" melts in olivine-hosted melt inclusions from the Gudchikhinsky Formation (Sobolev *et al.*, 2009) are also plotted for comparison. Compared with the uncontaminated Gudchikhinsky melt inclusions (which have La/Yb ~ 5), the melt inclusions described in this study are, in general, more depleted. Figure 7a illustrates the remarkably flat REE patterns of the uncontaminated Gudchikhinsky melts in the LREE part of the spectrum, with a significant decline towards the HREE. In contrast, the melt inclusion compositions reported here have, in general, higher La/Sm and lower Sm/Yb ratios. Some of the melt inclusions are more enriched than the bulk-rock composition (shown in black), whereas others are more depleted. La/Yb in the melt inclusions ranges from 0·7 to 9·5, with a median of 2·4 versus 4·1 in the bulk dolerites (Fig. 7a). Principal component analysis (PCA) (see Discussion and Supplementary Data for more details) demonstrates that the first principal component is related to the uniform dilution or enrichment of trace elements, whereas the second principal component is associated with variation in the slope.

The melt inclusions are highly variable in their LILE contents, such as Ba, Rb, Sr and K, relative to Primitive Mantle (McDonough & Sun, 1995) (Fig. 7b). The multi-element patterns of the melt inclusions demonstrate distinctive negative Nb and P anomalies, which do not appear in the Gudchikhinsky melt inclusion patterns.

The volatile concentrations in the melt inclusions are mostly low, but variable, with <890 ppm CO_2, <510 ppm Cl, <850 ppm F and <510 ppm S (mostly < 300 ppm) (Table 3). The absolute concentrations of CO_2 are uniformly low, about 180 ppm on average (Table 3). The melt inclusions from our study are considerably poorer in volatiles than the primary Gudchikhinsky melts (Sobolev *et al.*, 2009). We consider the volatile systematics using volatile/refractory trace element ratios. Owing to their similar compatibility in the melt, changes in these ratios indicate either mantle source composition variability, crustal contamination or magma degassing, which depletes the volatile concentration. Ratios of the volatile elements to similarly compatible trace elements show a considerable range. F/Nd ratios range from 9 to 79; Cl/K from <0·005 to >0·07 and S/Dy from 6 to 126. Overall, the F/Nd ratio is significantly higher than expected for primitive mantle and mid-ocean ridge basalt (MORB), whereas S/Dy is considerably lower than expected. The melt inclusions are poor in sulfur, which does not correlate with any trace element. Uncontaminated Gudchikhinsky melts are also poor in sulfur, ranging from 300 to 500 ppm for a MgO content of 9·70–10·05 wt % (Sobolev *et al.*, 2009). The Cl/K ratios of the melts are mostly higher than for MORB (Cl/K ~0·03; Saal *et al.*, 2002), even though the absolute concentrations of Cl are relatively low (Table 3). Enrichment in Cl relative to K has also been observed in both olivine- and plagioclase-hosted melt inclusions from Ust-Ilimsk and Bratsk sills (Black *et al.*, 2012) and in the Gudchikhinsky melt inclusions (Sobolev *et al.*, 2009). The F/Nd ratio of the analysed melt inclusions extends up to 80 (Fig. 8b), which is far beyond the uniform value of 21 defined by oceanic basalts (Workman *et al.*, 2006) and observed for Siqueiros MORB (Saal *et al.*, 2002). Recent experiments by Rosenthal *et al.* (2015) suggest that partition coefficients for fluorine are more similar to those of La than Nd. The F/La ratios of the melt inclusions range up to 315, which much higher than for MORB.

DISCUSSION

Geochemistry of the Khakanchansky, Ayansky and Khonnamakitsky Formations

REE systematics of the whole-rock compositions are summarized in Fig. 9. The Khakanchansky Formation forms part of the first low-titanium sequence, together with the Tulkonsky and Nadezhdinsky Formations (Reichow *et al.*, 2005). The La/Sm ratios of the Khakanchansky lava flows vary from low (2·25) to high (4·92), whereas Sm/Yb is <1·92, in common with all magmas of the low-Ti magmatic series. Magmas with higher La/Sm, such as those of the Nadezhdinsky Formation, are thought to have experienced a high degree of crustal contamination (Reichow *et al.*, 2005), which is also reflected in high $^{87}Sr/^{86}Sr$ (0·70672–0·70872) and low εNd (–11 to –8·2 for the lower parts of the Nadezhdinsky Formation) (Wooden *et al.*, 1993). The Khakanchansky basalts, based on their relatively low La/Sm, appear to have experienced low or variable degrees of crustal contamination. The basalts of the

Table 2: Host clinopyroxene major element composition

Sample	CPx Mg# host	SiO_2	TiO_2	Al_2O_3	FeO_{tot}	MnO	MgO	CaO	Cr_2O_3	NiO	Na_2O	K_2O	Total
S10–19 mi1	79·13	51·96	0·00	2·77	7·96	0·24	16·93	18·69	0·54	0·21	0·20	0·02	99·52
S10–19 mi2	80·87	52·41	0·44	2·44	7·10	0·16	16·83	19·61	0·24	0·03			99·25
S10–19 mi3	79·51	52·29	0·48	2·61	7·54	0·20	16·41	19·72	0·14	0·03			99·41
S10–19 mi4	79·13	51·96	0·00	2·77	7·96	0·24	16·93	18·69	0·54	0·21	0·20	0·02	99·52
S10–19 mi5	80·91	51·92	0·00	2·34	7·09	0·32	16·85	19·88	0·45	0·10	0·16	0·00	99·11
S10–19 mi6	80·78	52·85	0·01	2·00	7·15	0·24	16·86	19·96	0·39	0·21	0·19	0·03	99·89
S10–19 mi7													
S10–19 mi8													
S10–19 mi9	79·80	52·25	0·00	1·50	7·44	0·06	16·48	19·80	0·39	0·19	0·17	0·01	98·28
S10–19 mi10	78·22	51·73	0·00	2·29	8·11	0·65	16·33	18·91	0·83	0·19	0·27	0·02	99·32
S10–19 mi11	82·45	52·71	0·01	2·18	6·41	0·27	16·89	20·53	0·40	0·18	0·18	0·02	99·78
S10–19 mi12	79·41	51·69	0·00	2·80	7·51	0·25	16·25	20·04	0·60	0·16	0·20	0·04	99·55
S10–19 mi13	80·11	52·98	0·00	1·67	7·49	0·14	16·91	19·91	0·38	0·30	0·15	0·00	99·92
S10–19 mi14	82·10	52·85	0·00	2·02	6·48	0·34	16·66	20·89	0·39	0·16	0·18	0·02	99·99
S10–19 mi15	79·55	52·95	0·00	2·02	7·36	0·11	16·06	20·22	0·47	0·15	0·18	0·01	99·53
S10–19 mi16	79·55	52·95	0·00	2·02	7·36	0·11	16·06	20·22	0·47	0·15	0·18	0·01	99·53
S10–19 mi17	79·88	52·76	0·02	2·02	7·29	0·11	16·24	20·44	0·47	0·20	0·19	0·03	99·76
S10–19 mi18	81·00	52·85	0·01	2·08	6·98	0·09	16·68	20·30	0·35	0·18	0·19	0·05	99·75
S10–19 mi19	79·72	52·22	0·01	2·29	7·58	0·19	16·72	19·83	0·43	0·15	0·17	0·01	99·60
S10–19 mi20	80·49	52·82	0·02	2·23	7·13	0·26	16·49	19·97	0·38	0·13	0·18	0·02	99·61
S10–3 mi1	77·47	51·28	1·03	2·76	8·17	0·21	15·75	19·17	0·80	0·02			99·19
S10–3 mi2	76·83	51·45	1·06	2·57	8·29	0·21	15·43	19·53	0·47	0·03			99·03
S10–3 mi3	73·50	51·97	0·00	1·87	9·63	0·44	14·98	19·13	0·98	0·24	0·27	0·02	99·54
S10–3 mi4	77·74	51·47	0·93	2·61	7·96	0·22	15·59	19·72	0·73	0·01			99·25
S10–3 mi5	78·84	51·65	0·87	2·64	7·52	0·22	15·71	19·61	0·80	0·02			99·02
S10–3 mi6	77·53	52·99	0·00	1·50	8·45	0·45	16·34	18·93	0·66	0·27	0·27	0·02	99·89
S10–3 mi7	78·30	52·96	0·00	1·60	8·17	0·62	16·53	18·61	0·62	0·18	0·23	0·06	99·57
S10–3 mi8	77·61	51·73	0·01	2·68	7·84	0·68	15·25	19·61	0·94	0·22	0·28	0·01	99·24
S10–3 mi9	77·41	52·68	0·68	1·52	8·79	0·21	16·90	18·15	0·48	0·02			99·42
S10–3 mi10	78·17	51·84	0·83	2·44	8·05	0·23	16·17	19·15	0·75	0·01			99·47
S10–3 mi11	77·56	51·55	0·98	2·41	8·09	0·23	15·68	19·73	0·58	0·04			99·28
S10–3 mi12	76·18	52·40	0·00	2·00	8·57	0·36	15·37	19·40	0·87	0·22	0·26	0·04	99·49
S10–3 mi13	78·75	52·75	0·65	1·59	7·97	0·22	16·56	19·05	0·48	0·02			98·82
S10–3 mi14	78·12	52·55	0·65	1·50	8·45	0·19	16·91	18·62	0·39	0·03			99·28
S10–3 mi15	72·54	51·25	1·20	2·96	10·12	0·25	14·99	17·69	0·10	0·02			98·57
S10–3 mi16	77·10	52·90	0·00	1·41	8·78	0·48	16·58	18·05	0·65	0·23	0·21	0·03	99·32
S10–3 mi17													
S10–3 mi18	78·74	51·72	19·47	2·56	7·68	0·76	15·95	0·01	0·83	0·18	0·29	0·03	99·46
S10–3 mi19	76·14	52·14	18·72	1·98	9·00	0·24	16·11	0·00	0·85	0·22	0·26	0·04	99·54
S10–3 mi20	82·09	52·99	20·61	1·85	6·51	0·21	16·73	0·00	0·39	0·17	0·20	0·02	99·69
S10–3 mi21	79·99	52·97	19·84	1·46	7·56	0·08	16·95	0·00	0·37	0·18	0·18	0·03	99·61
S10–44 mi1	69·22	52·38	17·75	1·62	11·85	0·03	14·95	0·02	0·62	0·28	0·27	0·02	99·80
S10–44 mi2	71·93	51·49	20·37	2·24	9·65	0·27	13·87	0·00	0·87	0·24	0·29	0·01	99·32

Oxides and total are in wt %. Average of 3–4 points analysed around each melt inclusion.

Ayansky and Khonnamakitsky Formations belong to the upper low-titanium sequence (Reichow *et al.*, 2005). Samples from these formations are characterized by La/Sm ranging from 2·19 to 2·97 and Sm/Yb ranging from 1·21 to 1·33, similar to those from the Morongovsky Formation (Fig. 9). Most of the Khonnamakintsky sills have low La/Sm and Sm/Yb ratios, similar to those of the Mokuaevsky, Khraelakhsky and Kumingsky Formations of the upper series and the Samoedsky Formation, which is thought to represent the top of the magmatic sequence (Hawkesworth *et al.*, 1995; Reichow *et al.*, 2005). Two sills (samples S10–48 and S10–62) were probably contaminated by continental crust, with La/Sm ratios in the field of those for the Nadezhdinsky Formation, which is highly contaminated by continental crust. Notably, samples targeted here for their melt inclusions (encircled in red on Fig. 9) are clearly not contaminated significantly by continental crust.

Gudchikhinsky magmas are characterized by low La/Sm ratios (1·81–2·77) and high Sm/Yb (2·16–2·49), combined with low $^{87}Sr/^{86}Sr$ (0·70571–0·70678) and high εNd (from +1·9 to +4·2). These magmas belong to the early high-titanium series (Fig. 2) and are believed to be purely pyroxenite-derived (Sobolev *et al.*, 2011). In contrast, magmas of the Ivakinsky and Syverminsky Formations are contaminated by continental crust, reflected in their higher La/Sm and lower εNd (from –0·2 to –3·4) (Wooden *et al.*, 1993).

Petrogenetic relationships between crystals and whole-rocks

Melt inclusions were analysed in clinopyroxene macrocrysts. The macrocrysts may be phenocrysts (i.e. in equilibrium with the whole-rock) or antecrysts (entrained from disaggregating crystal mushes and out of equilibrium with the whole-rock). To assess whether the

Table 3: Major and trace element compositions of clinopyroxene-hosted melt inclusions and host clinopyroxenes

Sample:	Cpx-hosted melt inclusions							
	S10–19							
	mi1	mi2	mi3	mi4	mi5	mi6	mi7	mi8
Mg# host	79·13	80·87	79·51	79·13	80·91	80·78	*	*
SiO_2, wt %	50·95	46·16	47·27	50·06	49·89	50·60	49·86	51·24
TiO_2	0·46	1·02	0·83	0·24	0·29	0·64	0·34	0·42
Al_2O_3	7·36	2·29	15·46	13·69	11·85	14·06	12·82	10·79
FeO_{tot}	7·78	20·52	8·78	10·56	14·18	9·78	12·55	14·37
MnO	0·15	0·33	0·15	0·11	0·19	0·21	0·24	0·21
MgO	13·49	10·74	9·54	8·29	8·87	8·34	8·96	8·77
CaO	17·36	14·10	13·10	13·52	12·74	13·49	12·97	12·32
Na_2O	0·86	0·63	1·48	1·65	1·60	1·82	1·57	1·76
K_2O	0·12	0·20	0·21	0·12	0·14	0·20	0·12	0·13
P_2O_5	0·04	0·07	0·07	0·00	0·04	0·01	0·06	0·03
Total	98·56	96·05	96·89	98·24	99·77	99·16	99·49	100·04
F, ppm	202·17	307·11	−5·23	286·39	52·43	77·32	337·26	89·93
S	37·59	268·43	−7·78	56·66	85·41	61·71	70·78	41·26
Cl	83·00	476·50	101·00	*	*	11·00	*	*
CO_2	*	*	567·70	*	53·65	*	199·48	*
Ni	54·23	334·76	40·08	235·80	282·17	33·80	40·87	62·88
Cr	1721·63	18220·18	756·05	379·62	516·42	393·98	242·82	182·63
Hf	0·63	1·49	1·25	0·44	0·99	0·93	0·73	1·38
Sr	69·67	63·81	140·61	68·06	121·98	24·77	89·28	136·29
Y	10·29	13·17	17·97	8·72	10·38	12·16	12·24	22·65
Zr	17·37	53·63	39·29	14·08	20·98	11·62	25·89	61·32
Nb	0·26	3·42	2·20	0·32	0·50	0·09	0·81	2·62
Ba	13·62	87·96	66·79	9·25	15·35	7·10	19·02	78·27
La	*	6·28	*	1·11	1·40	1·08	2·91	6·87
Ce	*	12·38	*	2·81	3·47	3·37	6·59	14·78
Pr	*	1·64	*	0·39	0·51	0·57	1·05	2·06
Nd	*	8·41	*	2·68	2·79	3·94	5·74	9·48
Sm	*	1·87	*	0·89	0·88	1·35	1·83	2·33
Eu	*	0·58	*	0·37	0·33	0·51	0·49	0·91
Gd	*	1·88	*	1·27	1·94	2·54	1·91	3·81
Tb	*	0·35	*	0·21	0·23	0·33	0·36	0·64
Dy	*	2·12	*	1·20	1·95	2·23	2·00	4·18
Ho	*	0·54	*	0·28	0·37	0·42	0·44	0·86
Er	*	1·36	*	0·95	1·39	1·30	1·33	2·12
Tm	*	0·18	*	0·17	0·23	0·21	0·24	0·35
Yb	*	1·69	*	1·13	1·59	1·55	1·48	2·20
Lu	*	0·25	*	0·14	0·27	0·16	0·25	0·32

crystals were produced from the melts during equilibrium crystallization, we plot the Mg-number of the whole-rocks (which may approximate the bulk melt composition) versus the Mg-number of the clinopyroxene microphenocrysts contained within them (Fig. 5). The Fe–Mg distribution coefficient between clinopyroxene and liquid in equilibrium [$K_D^{Fe-Mg} = (Mg^{Liq}Fe^{Cpx})/(Mg^{Cpx}Fe^{Liq})$] is $0{\cdot}275 \pm 0{\cdot}067$ (Putirka *et al.*, 2003), which is temperature independent. The Mg-number of the whole-rock is defined as the molar ratio 100MgO/(MgO + FeO), assuming $FeO/FeO_{tot} = 0{\cdot}9$. The differences between the Mg-number of the bulk-rocks (53·4–55·9) and those of their clinopyroxene phenocrysts (69·2–82·5; Fig. 5) broadly reflects equilibrium, suggesting that the pyroxenes are not antecrysts. Most of the analysed clinopyroxene hosts to melt inclusions are in equilibrium with the whole-rock, whereas those lying below the curve can be attributed to closed-system differentiation (Putirka, 2008) and accumulation of mafic minerals, the latter resulting in elevated whole-rock Mg#.

Melt inclusion geochemistry

Below we discuss the major processes responsible for the compositions of the melt inclusions. We begin by summarizing the main features of their geochemistry and discuss the provenance of the melts with respect to their crystal hosts and the whole-rock composition. We then discuss the following as potential factors in their petrogenesis: (1) the role of mantle heterogeneity in the generation of these melts, evaluating the role of mixed peridotite–pyroxenite sources in generating some of the distinctive trace element chemistry; (2) crustal contamination; (3) evaporite assimilation; (4) the potential involvement of a fluid phase. Lastly, we discuss our findings in the context of the volatile output of the Siberian Traps volatile output and associated environmental impacts.

Principal component analysis (PCA) reveals the main controls on melt inclusion geochemistry. The first principal component elevates all the incompatible trace elements and volatiles to the same extent (see

Table 3: Continued

Sample:	Cpx-hosted melt inclusions							
	S10–19							
	mi9	mi10	mi11	mi12	mi13	mi14	mi15	mi16
Mg# host	79·80	78·22	82·45	79·41	80·11	82·10	79·55	79·55
SiO_2, wt %	50·13	53·18	49·81	50·49	51·78	49·22	50·40	50·34
TiO_2	0·27	1·03	0·27	0·35	0·34	0·32	0·70	0·65
Al_2O_3	13·32	13·59	14·21	13·99	14·07	10·34	13·24	13·41
FeO_{tot}	11·03	7·72	9·84	10·25	9·17	15·40	10·22	10·16
MnO	0·17	0·15	0·16	0·21	0·17	0·22	0·16	0·16
MgO	8·49	7·87	8·36	8·99	8·57	8·89	8·50	8·76
CaO	13·60	12·00	13·71	12·97	12·71	12·14	13·12	13·16
Na_2O	1·69	2·08	1·80	1·74	1·83	1·58	1·69	1·67
K_2O	0·17	0·47	0·12	0·15	0·33	0·18	0·15	0·15
P_2O_5	0·00	0·21	0·03	0·04	0·05	0·00	0·09	0·02
Total	98·88	98·30	98·31	99·18	99·02	98·28	98·26	98·48
F, ppm	108·61	19·39	118·83	162·48	23·25	71·79	5·29	2·58
S	59·89	66·39	55·28	125·00	22·50	202·79	69·82	50·79
Cl	*	*	*	67·00	*	*	67·00	*
CO_2	4·99	6·50	*	36·80	2·00	9·18	2·56	*
Ni	20·44	68·38	0·00	187·85	47·95	271·17	0·00	80·96
Cr	225·04	859·10	397·40	410·40	264·02	303·70	138·17	121·07
Hf	0·32	1·29	0·31	0·35	0·56	1·13	1·11	0·98
Sr	57·16	167·22	151·10	108·46	155·43	60·60	129·82	150·54
Y	9·04	19·45	5·83	9·53	10·35	11·21	13·50	14·15
Zr	18·35	49·58	13·03	15·55	20·93	65·08	31·28	36·35
Nb	0·54	2·18	0·39	0·30	0·92	1·14	1·44	1·70
Ba	17·83	57·24	23·21	24·06	59·51	10·11	41·43	46·90
La	1·49	5·34	*	1·51	2·80	1·82	3·32	3·76
Ce	3·67	12·93	*	3·73	6·18	4·28	7·40	7·66
Pr	0·65	1·85	*	0·50	0·83	0·62	0·98	1·13
Nd	2·68	11·20	*	3·50	4·03	3·40	5·64	5·80
Sm	1·28	3·32	*	0·91	1·15	1·21	1·69	1·77
Eu	0·58	0·98	*	0·52	0·62	0·39	0·59	0·70
Gd	1·62	3·25	*	1·56	1·72	1·14	1·99	2·11
Tb	0·31	0·64	*	0·27	0·40	0·35	0·33	0·37
Dy	1·70	4·37	*	1·91	1·79	1·75	2·32	2·82
Ho	0·36	0·79	*	0·36	0·37	0·43	0·53	0·54
Er	1·11	2·04	*	1·03	1·46	1·07	1·35	1·33
Tm	0·13	0·33	*	0·16	0·20	0·17	0·22	0·23
Yb	1·01	2·04	*	0·97	1·33	1·48	1·40	1·67
Lu	0·16	0·28	*	0·15	0·15	0·21	0·25	0·24

Supplementary Data), with variation related to crystal fractionation (75% of total variance; see Supplementary Data for a more detailed explanation). The major element geochemistry is dominated by trends arising from the fractionation of pyroxene and plagioclase. The melt inclusions span a large range of compositions, from primitive basalt to andesite; the latter is considerably more evolved than the bulk-rock composition, which is basaltic.

The second most important factor, according to the PCA, is a mantle melting signature that controls the slope of the REE pattern. Together these two principal components account for more then 90% of the variance in the melt inclusion geochemistry, which suggests that crustal contamination (and post-entrapment modification) is not a dominant geochemical control, because this process would generate distinctive covariances between sets of trace elements that are not observed in the dataset. The trace element compositional profiles of the melt inclusions show overall more depleted REE abundances relative to the "primary" olivine-hosted melt inclusions reported by Sobolev *et al.* (2009), suggesting that these melts are derived by large degrees of melting of a source composed of dominantly peridotite, with a small amount of halogen-rich pyroxenite. The primary melts were relatively depleted in incompatible elements, including volatiles, with the absolute concentrations of sulfur, chlorine and fluorine being lower than in primary melts derived by smaller degrees of melting of peridotite. Halogens are relatively enriched with respect to similar refractory trace elements, however, perhaps as a result of halogen-rich pyroxenite in the source.

Relationship between melt inclusions, the carrier liquids and their crystal hosts

The diversity of melt inclusion compositions relative to that of the bulk magma and the carrier liquid (matrix glass) is shown in Fig. 7. This is a feature observed in many ocean island basalts, MORB and continental basalts worldwide (Maclennan *et al.*, 2003; Danyushevsky,

Table 3: Continued

Sample:	Cpx-hosted melt inclusions							
	S10–19				S10–3			
	mi17	mi18	mi19	mi20	mi1	mi2	mi3	mi4
Mg# host	79·88	81·00	79·72	80·49	77·47	76·83	73·50	77·74
SiO_2, wt %	49·83	50·22	49·75	48·34	51·17	54·97	55·49	52·48
TiO_2	0·61	0·48	0·53	0·34	0·72	0·69	2·13	0·57
Al_2O_3	13·12	14·23	14·55	14·63	10·82	14·60	11·50	13·63
FeO_{tot}	11·48	9·27	9·63	9·50	12·75	7·63	8·92	9·14
MnO	0·25	0·19	0·20	0·14	0·27	0·03	0·13	0·14
MgO	8·41	7·71	8·07	8·22	7·36	7·53	6·20	7·53
CaO	13·21	14·69	14·02	13·82	11·82	13·52	8·56	12·89
Na_2O	1·75	1·85	2·01	1·64	1·89	2·51	2·69	2·28
K_2O	0·22	0·24	0·18	0·22	0·36	0·36	2·12	0·79
P_2O_5	0·06	0·13	0·00	0·07	0·03	0·06	0·31	0·05
Total	98·93	99·02	98·95	96·92	97·20	101·90	98·05	99·51
F, ppm	33·26	47·74	64·65	27·12	4·00	34·83	481·33	146·52
S	114·70	66·62	23·30	113·74	177·56	52·31	437·65	24·94
Cl	*	62·00	47·00	66·00	45·00	*	39·00	3·00
CO_2	627·55	*	374·75	*	*	33·67	891·67	50·50
Ni	110·83	0·00	0·00	231·87	0·00	0·00	211·43	109·23
Cr	612·18	253·08	312·59	474·70	6747·68	1204·21	427·50	1440·95
Hf	0·97	1·00	0·38	0·91	1·34	1·86	2·18	1·22
Sr	105·35	349·50	211·95	111·14	189·66	*	71·15	237·64
Y	14·77	17·26	4·61	9·20	17·00	*	21·46	13·99
Zr	46·34	42·84	13·00	27·89	34·31	36·81	73·10	28·02
Nb	1·81	1·85	0·72	0·87	0·97	1·54	4·61	0·65
Ba	51·11	72·32	34·20	26·13	40·00	82·67	89·71	61·11
La	4·33	7·56	2·14	1·86	2·97	4·04	7·37	3·28
Ce	9·21	14·88	4·28	4·17	7·75	9·40	17·41	8·27
Pr	1·37	1·88	0·54	0·65	1·38	1·40	2·37	1·28
Nd	6·53	10·15	2·46	3·19	9·05	8·49	12·78	7·32
Sm	1·75	2·46	0·70	1·09	2·18	1·93	4·22	1·83
Eu	0·66	0·80	0·36	0·42	0·86	0·92	1·19	0·91
Gd	2·25	2·78	0·59	1·33	2·52	2·41	4·52	2·20
Tb	0·38	0·49	0·10	0·22	0·49	0·50	0·69	0·44
Dy	2·58	2·92	0·83	1·23	3·34	2·76	4·35	2·75
Ho	0·59	0·64	0·18	0·33	0·63	0·69	0·88	0·54
Er	1·50	2·12	0·50	0·94	2·10	1·62	1·94	1·87
Tm	0·25	0·24	0·08	0·18	0·31	0·23	0·30	0·28
Yb	1·48	1·99	0·44	1·10	2·13	1·92	1·99	1·77
Lu	0·26	0·26	0·08	0·15	0·25	0·18	0·34	0·25

2004; Kent, 2008). Magma mixing diminishes the compositional variations during or after melt entrapment and therefore a larger range of melt compositions is retained in the melt inclusions (Sobolev & Shimizu, 1993; Nielsen *et al.*, 1995; Kent, 2008). The trapped melts have also undergone variable amounts of crystal fractionation, as illustrated by major element trends versus decreasing host clinopyroxene Mg# (Fig. 6). All these factors combined lead to geochemically diverse melt inclusion compositions.

Mantle heterogeneity and degree of melting

Previous studies have considered the influence of lithological variations in mantle source regions on the geochemical composition of the melts being produced (Sobolev *et al.*, 2005, 2007; Herzberg, 2006; Shorttle & Maclennan, 2011). To track the influence of SLIP mantle source heterogeneity (Sobolev *et al.*, 2009, 2011) on the trace element characteristics of the melts we have modelled the melting of two potential mantle source components: peridotite and pyroxenite. The pMELTS model was used to calculate the major and trace element composition of accumulated fractional melts produced by isentropic, adiabatic decompression of peridotite and pyroxenite with modelling performed with the alphaMELTS software (Ghiorso *et al.*, 2002; Smith & Asimow, 2005). Peridotite compositions KLB-1 (Takahashi, 1986) and depleted MORB mantle (DMM) (Workman & Hart, 2005) were used for the starting major and trace element compositions, respectively. The pyroxenite major element starting composition in the model was hybrid Px-1, which has been proposed to guarantee a stable pyroxenite lithology (Sobolev *et al.*, 2007). Estimates of trace element concentrations were based on the approach described by Rudge *et al.* (2013); that is, binary mixing of DMM (Workman & Hart, 2005) and bulk subducted igneous crust in equal proportions. The subducted oceanic crust was assumed to contain 25% altered MORB, 25% fresh normal (N)-MORB and 50% gabbro, as proposed by Stracke *et al.* (2003). The starting temperature and pressure were assumed to be 1500°C and 4 GPa, which are consistent

Table 3: Continued

Sample:	Cpx-hosted melt inclusions							
	S10–3							
	mi5	mi6	mi7	mi8	mi9	mi10	mi11	mi12
Mg# host	78·84	77·53	78·30	77·61	77·41	78·17	77·56	76·18
SiO_2, wt %	51·02	54·12	52·89	51·08	50·46	51·66	48·93	50·04
TiO_2	0·50	1·81	1·75	0·59	0·45	0·49	0·59	0·66
Al_2O_3	14·10	10·59	9·80	14·70	15·01	14·90	12·40	13·20
FeO_{tot}	9·75	9·31	9·62	8·59	8·58	9·47	12·47	9·83
MnO	0·21	0·20	0·18	0·15	0·19	0·25	0·19	0·23
MgO	7·94	7·55	7·63	7·56	7·80	7·66	8·99	7·92
CaO	12·85	9·80	10·15	13·36	13·30	13·66	12·32	12·96
Na_2O	2·21	2·78	1·92	1·89	2·24	2·08	1·81	1·85
K_2O	0·79	1·27	1·43	0·42	0·37	0·55	0·46	0·39
P_2O_5	0·02	0·44	0·22	0·06	0·01	0·01	0·04	0·12
Total	99·38	97·86	95·58	98·40	98·41	100·72	98·20	97·20
F, ppm	−2·13	8·45	135·26	43·32	50·87	848·46	19·01	16·54
S	36·21	38·15	268·13	97·27	2·75	32·56	43·15	68·38
Cl	55·00	53·00	71·00	45·00	*	*	*	*
CO_2	109·15	*	60·14	3·55	*	348·18	*	70·71
Ni	121·01	249·95	514·83	0·00	0·00	269·53	237·31	327·76
Cr	1260·32	502·06	3033·54	1072·51	264·79	1224·74	1687·95	276·34
Hf	1·06	5·75	1·01	1·15	1·18	1·22	1·37	0·88
Sr	272·85	267·05	28·81	247·68	178·57	225·89	269·37	281·88
Y	12·73	32·82	17·96	13·54	12·65	15·53	20·32	13·77
Zr	27·73	219·30	24·56	21·93	22·82	21·80	29·11	25·09
Nb	1·07	17·15	0·55	0·39	0·70	0·46	0·78	1·11
Ba	112·30	275·83	8·86	54·74	49·42	87·32	96·49	90·61
La	4·44	28·70	2·49	2·66	*	4·64	12·25	3·81
Ce	10·10	59·17	7·39	7·63	*	11·14	27·18	9·94
Pr	1·57	7·21	1·37	1·14	*	1·51	3·80	1·40
Nd	8·28	31·92	8·16	7·33	*	9·23	15·84	6·41
Sm	2·34	6·78	2·70	1·95	*	2·93	4·36	2·63
Eu	0·93	2·39	0·87	0·94	*	1·14	1·40	0·94
Gd	1·88	7·05	4·08	3·58	*	2·76	3·69	2·66
Tb	0·43	1·09	0·58	0·51	*	0·46	0·79	0·43
Dy	2·53	6·07	3·74	2·60	*	2·23	4·70	2·81
Ho	0·61	1·38	0·79	0·56	*	0·62	0·82	0·51
Er	1·23	3·47	2·07	1·53	*	1·83	1·97	1·64
Tm	0·22	0·44	0·28	0·22	*	0·23	0·29	0·23
Yb	1·73	3·02	1·85	1·10	*	1·49	2·21	1·52
Lu	0·18	0·46	0·29	0·15	*	0·21	0·34	0·20

with previous mantle potential temperature and depth of melting assessments (i.e. 1500–1580°C and 130–180 km; Sobolev *et al.*, 2009).

To track volatile/trace element ratios during melting we used partition coefficients for F and Cl in clino- and orthopyroxene from Dalou *et al.* (2014), and for olivine and garnet from Hauri *et al.* (2006), which were also used by Rosenthal *et al.* (2015). We assume initial F and Cl contents in peridotite of 16 and 0·83 ppm, respectively, based on MORB concentrations (Saal *et al.*, 2002). Pyroxenite is assumed to contain 140 ppm Cl, based on the assumption that the uncontaminated purely pyroxenite-derived melts of the Gudchikhinsky Formation represent a 0·4 melt fraction, and 280 ppm F, based on a F/Cl ratio of around two in EM2-sourced Society Islands melts (Kendrick *et al.*, 2014). We illustrate the paths of liquid composition evolution during melting based on the parameters mentioned above (Fig. 8).

To address the specifics of the Siberian Traps melts we plot Gd/Yb versus Ti/Y (Fig. 10). The high-Ti melt inclusion compositions (Ti/Y > 500) with high Gd/Yb > 3 are believed to be controlled by residual garnet in the source and represent melts of the pyroxenite component, whereas low Ti/Y and Gd/Yb ratios are attributed to higher degrees of melting of shallower peridotite (e.g. Xu *et al.*, 2001; Kamenetsky *et al.*, 2012). Pyroxenite-derived high-Ti Gudchikhinsky melts have high Gd/Yb of ~3 (Fig. 10; Sobolev *et al.*, 2009). Most of the analysed melt inclusions have low Gd/Yb (<2) and low Ti/Y (<300), defining a positive correlation between these two ratios. Compositions plotting outside this trend suggest that other processes exert a control on dominantly peridotite-sourced melts. Continuous mixing of peridotite (low Gd/Yb and Ti/Y) and pyroxenite (high Gd/Yb and Ti/Y) components is not capable of explaining the extreme values of La/Yb (>9 and ~1) in the melts. The assimilation of siliceous crustal material, such as the extremely enriched Bolgokhtoksky granodiorite (Hawkesworth *et al.*, 1995), is required to explain high Gd/Yb ratios at low Ti/Y (Fig. 10) This may also explain the very high La/Yb ratios in a few of the samples (e.g. S10–3 mi 6, 8, 15). The concentrations of HREE and HFSE in evaporites are

Table 3: Continued

Sample:	Cpx-hosted melt inclusions							
	S10–3							
	mi13	mi14	mi15	mi16	mi17	mi18	mi19	mi20
Mg# host	78·75	78·12	72·54	77·10	*	78·74	76·14	82·09
SiO_2, wt %	51·40	51·78	52·72	56·15	49·85	50·95	51·59	49·13
TiO_2	0·54	1·19	0·93	1·39	0·45	0·49	0·52	0·27
Al_2O_3	12·28	13·51	14·01	11·10	14·34	14·93	15·30	13·70
FeO_{tot}	9·92	8·82	8·30	8·12	8·83	8·50	7·45	11·25
MnO	0·19	0·18	0·20	0·17	0·15	0·15	0·19	0·20
MgO	8·47	7·72	7·76	6·80	7·49	8·06	7·26	8·61
CaO	12·68	12·13	12·95	9·15	12·89	12·64	13·51	13·58
Na_2O	1·40	2·26	2·28	2·95	2·39	2·32	2·71	1·64
K_2O	0·42	0·79	0·73	1·73	0·26	0·73	0·70	0·11
P_2O_5	0·00	0·18	0·09	0·29	0·03	0·05	0·03	0·07
Total	97·29	98·55	99·97	97·83	96·67	98·81	99·26	98·55
F, ppm	298·24	144·72	272·14	607·91	764·64	45·69	33·26	209·64
S	35·63	52·98	43·82	510·66	63·32	41·88	10·45	157·84
Cl	*	*	*	169·00	*	45·00	*	4·00
CO_2	802·48	783·27	29·93	86·72	24·50	*	3·83	1·13
Ni	0·00	0·00	139·87	0·00	45·59	0·00	35·37	343·48
Cr	847·05	552·84	280·53	718·20	638·17	1575·25	283·86	465·80
Hf	1·33	0·99	1·83	1·60	0·53	0·73	0·69	0·34
Sr	155·56	328·69	307·48	67·72	296·76	324·18	466·16	16·97
Y	15·92	11·60	19·93	19·13	9·00	10·37	7·47	9·69
Zr	25·56	26·25	38·39	51·30	18·25	19·58	17·59	8·69
Nb	0·52	1·22	1·95	3·43	0·84	0·90	0·59	0·10
Ba	55·82	100·28	116·43	65·87	87·35	96·87	121·86	1·24
La	2·47	3·94	7·95	5·88	2·42	3·58	2·93	*
Ce	7·90	9·33	16·77	13·16	6·09	8·66	6·62	*
Pr	1·29	1·21	2·35	1·85	0·94	1·31	0·87	*
Nd	8·72	6·76	12·83	10·69	4·47	6·39	4·55	*
Sm	2·47	1·79	3·25	2·87	1·52	1·40	1·47	*
Eu	0·91	0·77	1·35	0·83	0·91	1·08	0·92	*
Gd	2·36	1·98	4·47	4·25	1·72	1·93	1·43	*
Tb	0·59	0·43	0·69	0·66	0·31	0·34	0·27	*
Dy	3·36	2·07	4·03	4·03	1·61	2·03	1·65	*
Ho	0·70	0·50	0·91	0·81	0·40	0·37	0·30	*
Er	1·88	1·52	2·23	2·11	1·04	1·03	0·71	*
Tm	0·22	0·18	0·30	0·27	0·12	0·14	0·10	*
Yb	1·69	1·82	2·19	1·83	0·83	1·21	0·90	*
Lu	0·21	0·21	0·27	0·30	0·15	0·18	0·11	*

negligible (Pang *et al.*, 2013) and their assimilation could not produce the observed compositions.

Variable degrees of partial melting of pyroxenite (>30%) and peridotite (>10%) can broadly account for the chlorine and fluorine variations in the melt inclusions, according to our model predictions, as indicated by the arrows in Fig. 8b–d. The arrows show that the ratios change with progressive partial melting of peridotite and pyroxenite, respectively. Variations in Cl/K, F/Nd and F/La at a given value of La/Yb lie close to the model peridotite melting curves. The divergence in these ratios gravitates towards the pyroxenite melting curves. The sulfur concentrations in the melts are low and dominated by a degassing signature.

Crustal contamination and the role of a fluid-rich component

As demonstrated above, some of the geochemical diversity in melt inclusion compositions may be explained by mantle heterogeneity, except for the LILE enrichment, Nb minimum and volatile content variations. Fractionation and original heterogeneity within the primary melts of the mantle source (see above) have undoubtedly controlled a large amount of the diversity in melt inclusion geochemistry. Crustal contamination is perhaps almost inevitable during prolonged storage of large volumes of basaltic magma in the continental crust and has been shown to be a distinctive and important feature of many other continental flood basalts (Hawkesworth *et al.*, 1995; Devey & Cox, 1987; Brandon *et al.*, 1993; Baker *et al.*, 1996; Ewart *et al.*, 1998). Melt inclusions with a distinctive negative Nb anomaly probably represent melts contaminated by the continental crust (Fig. 7b), consistent with previous studies that have shown that Nb and Ti anomalies correlate with high concentrations of radiogenic Sr (Naldrett *et al.*, 1992; Lightfoot *et al.*, 1993; Fedorenko *et al.*, 1996; Reichow *et al.*, 2005).

The melt inclusions exhibit a range of Nb/Y ratios from 0·02 to 0·52, increasing towards higher La/Yb (Fig. 11). Some of the melt inclusion compositions may be accounted for by heterogeneous source melting (trend to high Nb/Y, high La/Yb), consistent with mixing between peridotite- and pyroxenite-derived melts,

Table 3: Continued

Sample:	Cpx-hosted melt inclusions			Cpx-host major and trace elements		
	S10–3	S10–44		S10–3	S10–19	S10–44
	mi21	mi1	mi2	mi3	mi17	mi2
Mg# host	79·99	69·22	71·93	73·50	79·88	71·93
SiO_2, wt %	49·80	48·95	44·13	51·97	52·76	51·49
TiO_2	0·34	3·03	2·02	0·98	0·47	0·87
Al_2O_3	14·21	8·81	10·34	1·87	2·02	2·24
FeO_{tot}	9·66	14·60	14·15	9·63	7·29	9·65
MnO	0·13	0·30	0·38	0·24	0·20	0·24
MgO	8·27	7·88	8·19	14·98	16·24	13·87
CaO	14·16	11·97	15·09	19·13	20·44	20·37
Na_2O	1·79	1·58	1·29	0·27	0·19	0·29
K_2O	0·18	0·71	0·35	0·00	0·02	0·00
P_2O_5	0·02	0·28	0·69	*	*	*
Total	98·56	98·11	96·63	99·08	99·63	99·04
F, ppm	207·65	380·71	1·18	*	*	*
S	181·59	267·38	161·66	*	*	*
Cl	53·00	511·00	54·00	*	*	*
CO_2	35·96	18·68	7·13	*	*	*
Ni	303·40	189·43	96·68	192·57	210·65	70·74
Cr	0·00	359·78	604·66	3039·70	725·72	1842·01
Hf	0·43	2·69	3·39	0·66	0·57	0·33
Sr	14·05	28·61	107·42	15·03	13·35	14·65
Y	9·32	25·97	29·55	14·91	15·64	12·93
Zr	6·71	85·18	127·19	13·01	11·60	9·44
Nb	0·04	2·19	14·67	0·10	0·02	0·10
Ba	1·08	45·14	126·56	0·17	0·17	0·21
La	*	4·14	13·90	0·46	0·99	0·41
Ce	*	10·84	27·40	2·28	2·78	2·04
Pr	*	1·63	3·49	0·42	0·61	0·40
Nd	*	9·81	16·63	3·33	4·34	2·66
Sm	*	2·87	3·82	1·53	1·61	1·54
Eu	*	0·69	1·54	0·54	0·63	0·40
Gd	*	3·41	4·86	2·12	2·28	2·36
Tb	*	0·60	0·80	0·36	0·42	0·34
Dy	*	4·91	5·39	2·91	2·84	2·44
Ho	*	1·00	1·13	0·56	0·57	0·55
Er	*	2·66	3·18	1·48	1·77	1·57
Tm	*	0·44	0·45	0·21	0·20	0·17
Yb	*	2·79	2·69	1·11	1·76	1·15
Lu	*	0·45	0·47	0·19	0·18	0·16

*not measured or below detection limit

whereas others show a smaller increase in Nb/Y with increasing La/Yb, which trends towards continental crust. Some melt inclusions show high Ba/La and Sr/La uncorrelated with any other elements (e.g. Cl, K, REE). These melts may have interacted with a component enriched in these elements, which could be a crustal fluid or a low-degree metasomatic melt (Fig. 12).

The role of crustal contamination in the formation of the SLIP has been previously addressed by a number of researchers (Lightfoot *et al.*, 1993; Fedorenko *et al.*, 1996; Reichow *et al.*, 2005). It is crucial to discriminate here between evaporite and siliceous crustal components. Assimilation of evaporites, both sulphate- and salt-dominated, will not influence melt REE enrichment (e.g. La/Yb ratio) owing to the very low concentrations of most REE in evaporites (Fig. 13a), but will substantially affect the volatile budget of the magmas (Fig. 13b–d). A siliceous crustal component, such as the extremely enriched Bolgokhtoksky granodiorite and also average continental crust, in contrast, will not contribute to the volatile content of melts (and will in fact dilute volatile concentrations) but could promote considerable melt enrichment in LILE and LREE. Crustal assimilation, if it was a key factor in the formation of these melts, would inevitably increase La/Yb ratios, which is not observed in most of the analysed melt inclusions (Fig. 8). The observed enhancement of Cl over K in the melt inclusions might be consistent with minor interaction with evaporites, as proposed by Black *et al.* (2012) for elsewhere in the province, but is also consistent with a small amount of chlorine-rich pyroxenite in the source (Fig. 8c), independently corroborated by the relatively high Ti/Y and Gd/Yb in a subset of the samples (Fig. 10), as previously proposed by Sobolev *et al.* (2009).

Implications of these results for the volatile budget of the SLIP

The overarching conclusions of our study are that those SLIP magmas erupted 400–800 kyr after the

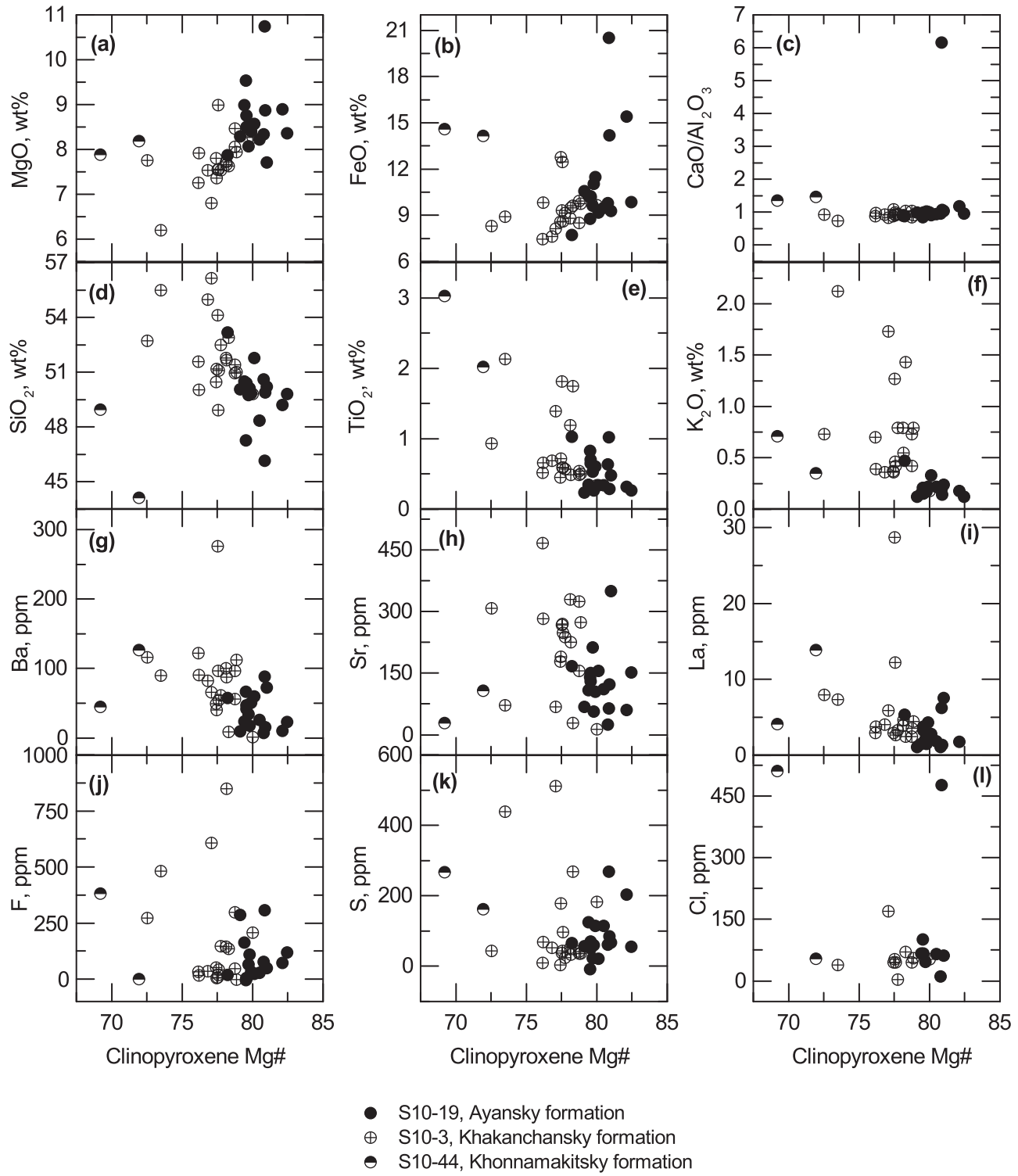

Fig. 6. Major (a–f) and trace (g–i) element and volatile (j–l) contents of melt inclusions vs Mg# of host clinopyroxene.

Gudchikinsky Formation magmas (which have been interpreted to be generated by pyroxenite melting) were the result of melting a source that had been depleted substantially in its pyroxenite component. The overall low concentrations of volatiles in the melts, which are consistent with the low concentrations of other incompatible trace elements, are a result of the melts having been formed by relatively large degrees (>15%) of peridotite melting. Relative enrichments in Cl and F with respect to refractory trace elements with similar partition coefficients suggest either that the pyroxenite component of the source, although minor in amount, was extremely halogen-rich or that the magmas interacted with evaporites in the subsurface (evaporites do not

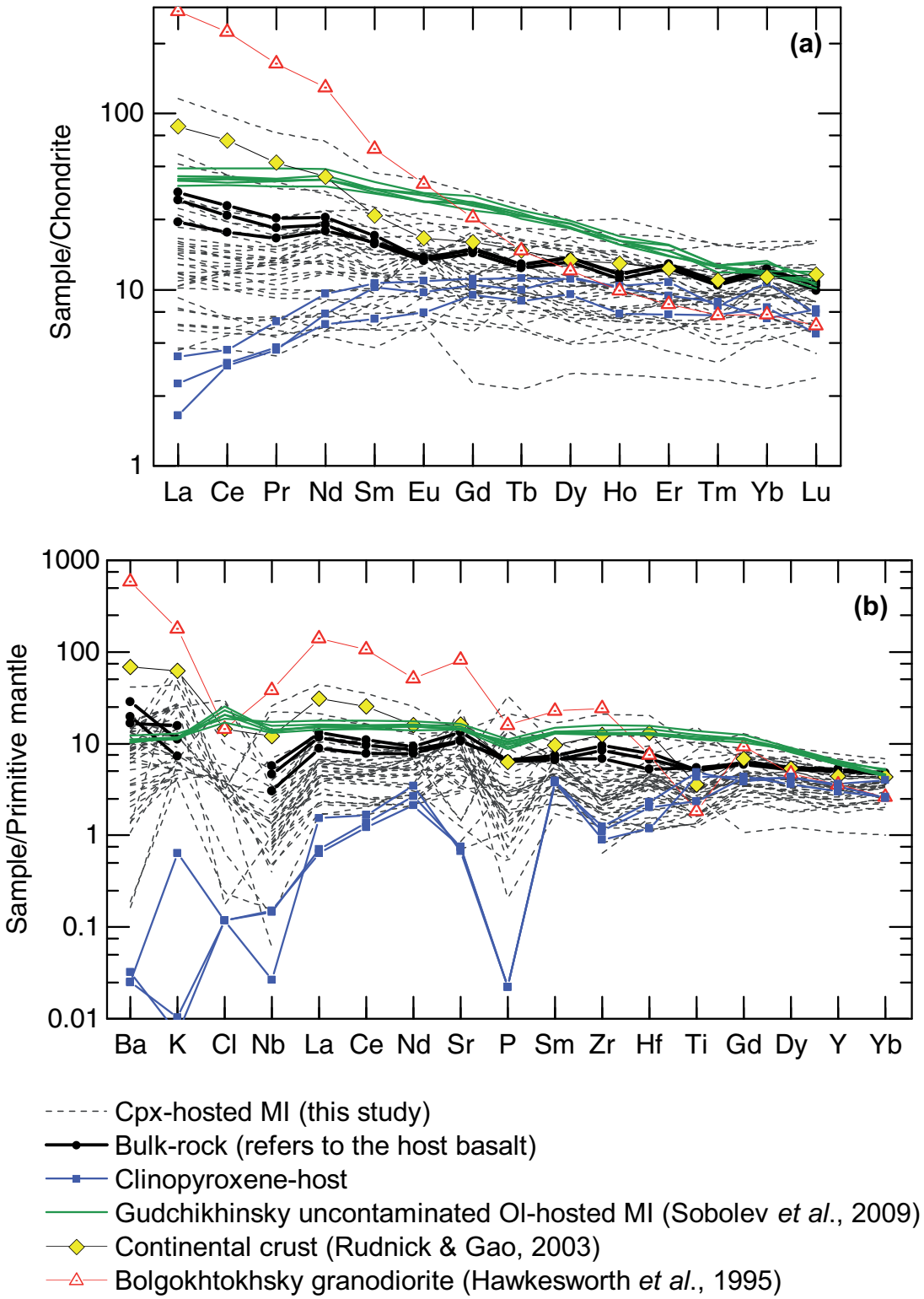

Fig. 7. (a) Rare earth and (b) multi-element patterns of analysed clinopyroxene-hosted melt inclusions from lava flows south of Norilsk, host clinopyroxenes, bulk-rock host basalt from which the clinopyroxene crystals were picked, average continental crust (Rudnick & Gao, 2003), Bolgokhtokhsky granodiorite (Hawkesworth *et al.*, 1995), and the most primitive uncontaminated melt inclusions from the Gudchikhinsky Formation (Sobolev *et al.*, 2009). Concentrations are normalized to the C1-chondrite values (Sun & McDonough, 1989) and Primitive Mantle values (McDonough & Sun, 1995), respectively.

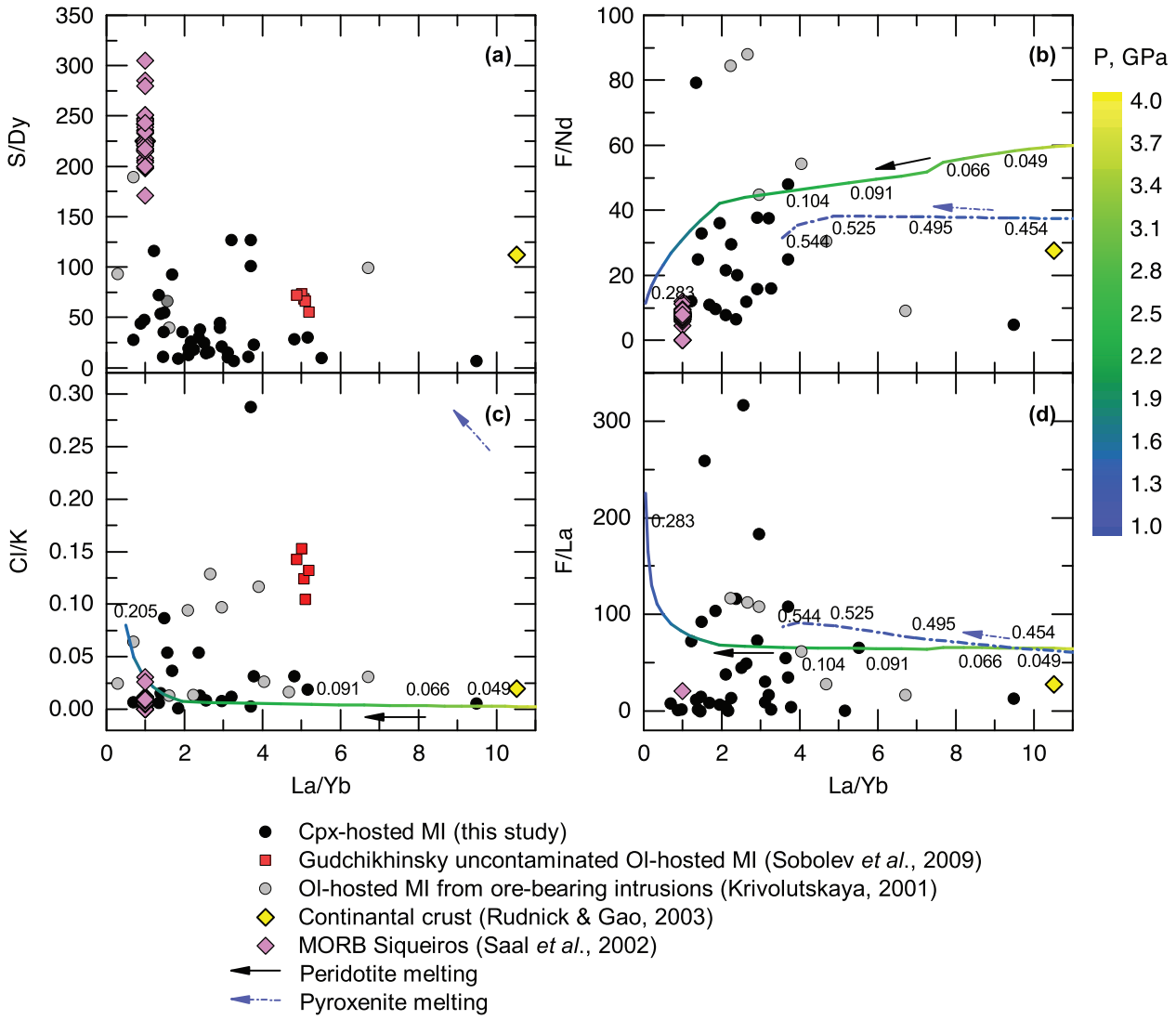

Fig. 8. Volatile/trace element ratios vs La/Yb in SLIP melt inclusions (MI) from this and other studies. Data sources: Gudchikhinsky Formation uncontaminated primitive melt inclusions, Sobolev *et al.* (2009); olivine-hosted MI from ore-bearing intrusions, Krivolutskaya (2001). Shown for comparison are data for Siqueiros MORB (Saal *et al.*, 2002) and average continental crust (Rudnick & Gao, 2003). Model melting curves for peridotite (continuous line) and pyroxenite (short dash–dot line) are colour-coded for pressure, varying from 4 to 1 GPa (see text for details).

form an outcrop or subcrop in the region). Other trace element indicators of pyroxenite involvement (e.g. elevated Ti/Y, Gd/Yb) suggest that this is the most likely explanation. Crustal contamination is relatively unimportant for these melts, but the overall effect of a small amount of contamination with siliceous crustal material is to dilute the incompatible elements in the melt, including the volatiles, further.

The volatile contents of the studied melt inclusions are low; furthermore, they are lower than those in the primary melts reported by Sobolev *et al.* (2009), which were interpreted to have been dominated by pyroxenite melting earlier in the Siberian Traps eruptive sequence. For sulfur and carbon, the low concentrations may be explained by pre-entrapment degassing, which is extremely common in melt inclusions in continental magmas. Chlorine and fluorine, on the other hand, are not expected to be modified significantly by degassing [owing to their greater solubilities in silicate melts (e.g. Webster, 2004, but their concentrations have certainly been modified by it (eradicating any correlations with other trace elements; Fig. 8). These magmas would contribute only around 20–50% of the magmatic gases sulfur dioxide, hydrogen chloride and carbon dioxide to the atmosphere compared with those supplied by the pyroxenite-derived magmas of Sobolev *et al.* (2009). This equates to ~70 ppm Cl in the analysed melt inclusions versus 350–400 ppm Cl for the primary melt inclusions of Sobolev *et al.* (2009) and, similarly, ~270 ppm S versus 350 ppm in the primary melts. The volatiles supplied to the atmosphere from large melt fractions of peridotite are also relatively small in magnitude

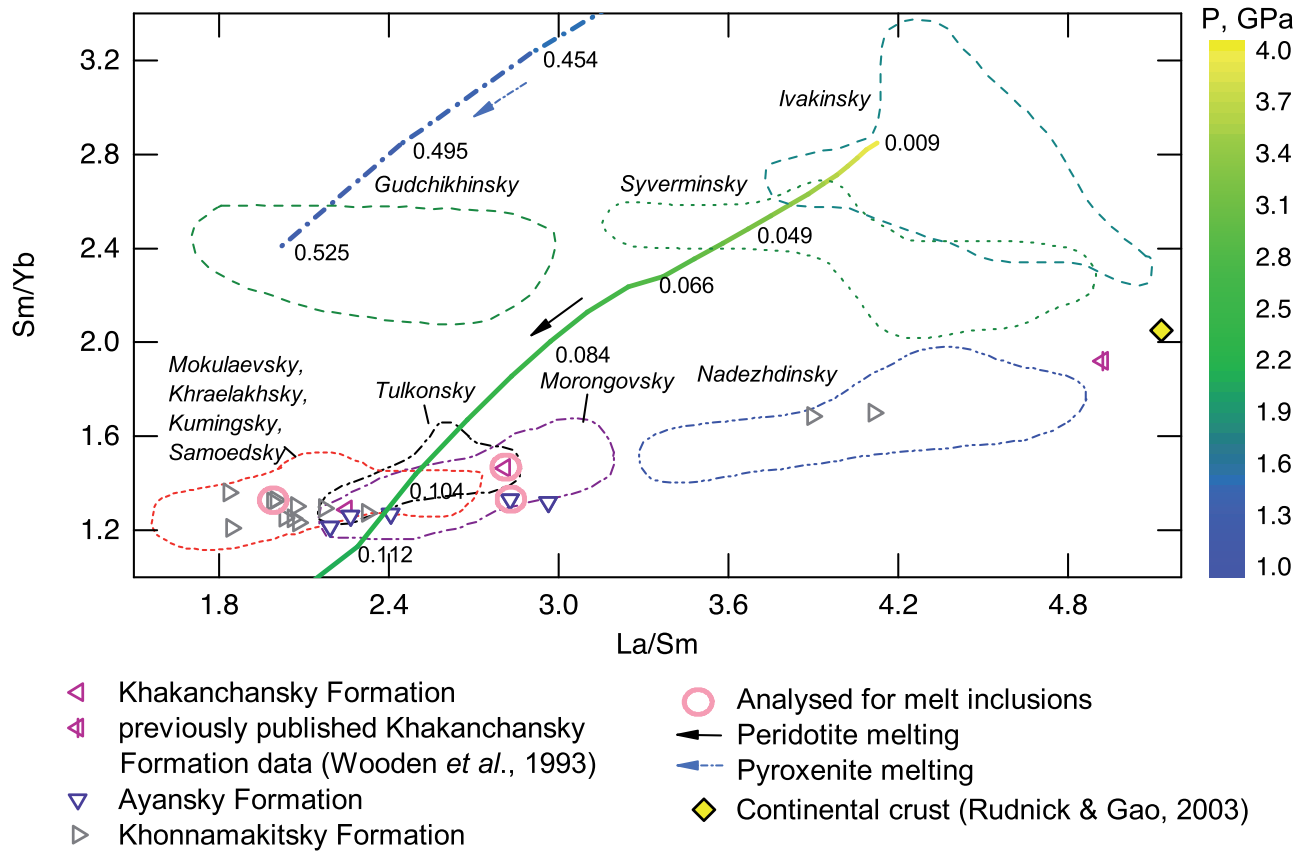

Fig. 9. La/Sm vs Sm/Yb for individual Siberian Traps formations. Data sources: Lightfoot *et al.* (1990, 1993); Wooden *et al.* (1993); Hawkesworth *et al.* (1995). Model curves for partial melting of peridotite (continuous line) and pyroxenite (short dash–dot line) are colour-coded for changing pressure from 4 to 1 GPa. Melt fractions are indicated. Samples analysed for melt inclusion composition are highlighted.

compared with those outgassed from magmas intruded into volatile-rich sediments (e.g. Svensen *et al.*, 2009; Black *et al.*, 2012) or from alkaline meimechite magmas (e.g. Black *et al.*, 2012). The reduced gaseous output from the magma does not, however, diminish the importance of degassing of volatile-rich country rocks owing to contact metamorphism and volatile release through venting structures (Svensen *et al.*, 2009; Aarnes *et al.*, 2010, 2011).

According to the most accurate existing estimates of the regional distribution of intrusions, lava flows and volcaniclastic material, the total volume of Siberian Traps magmas emplaced on the Siberian Craton is 1·75 million km^3 (Vasiliev *et al.*, 2000). Taking into account the lavas and sills that occur as subcrops in the West Siberian Basin, the total volume of the SLIP may be up to 4 million km^3 (Courtillot *et al.*, 1999; Fedorenko *et al.*, 2000). The volume of magmas not intruded directly into evaporites (but that could have interacted with them at depth) is up to about 590 000 km^3 [estimated based on the regional distribution of magmatic rocks in the SLIP reported by Vasiliev *et al.* (2000) compared with the known distribution of evaporites; Fig. 1], forming nearly one-third of the total magma volume on the Craton. The total volume of volatile-rich "'pyroxenite-derived'" melts of the high-Ti series is less than 25% of the total volume. The magmatic contribution to the volatile budget of the SLIP, if it is assessed based on extrapolating the compositions of volatile-rich melts from Norilsk (Sobolev *et al.*, 2009), the Maymecha–Kotuy Province (Black *et al.*, 2012) and the southern Cambrian evaporite region in the province (Black *et al.*, 2012; Tang *et al.*, 2013), may thus be highly overestimated. Assimilation of volatile-poor siliceous continental crustal material may have affected large volumes of the low-Ti series magmas, which were dominantly derived from a peridotite source (Fig. 2; Reichow *et al.*, 2005), which would serve to further dilute their volatile concentrations. It is presumed that the magmas enplaced in the West Siberian Basin were largely peridotite-derived, similar to the samples studied here. This means that about two-thirds of the Siberian Trap magmas, taking into account those in the West Siberian Basin, may have been poorer in volatiles compared with the volatile-rich melts analysed by Sobolev *et al.* (2009) and Black *et al.* (2012), which should be taken into account in volatile budget estimations.

Figure 14 shows a schematic illustration of the gaseous magmatic output of the SLIP over time, incorporating our interpretation of mantle source evolution. The first intensive volatile output, which occurred

before the main pulse of magmatism, came from purely pyroxenite-sourced magmas, which were rich in volatiles (particularly chlorine and carbon species; Sobolev *et al.*, 2009, 2011). With time, the pyroxenite component in the heterogeneous mantle source became exhausted and the source eventually became dominated by peridotite. The melt inclusions reported in our current study preserve a signature suggesting a small proportion of pyroxenite component in the source (see discussion above). According to the latest geochronology studies (Kamo *et al.*, 2003; Song *et al.*, 2012; Burgess *et al.*, 2014; Burgess & Bowring, 2015),

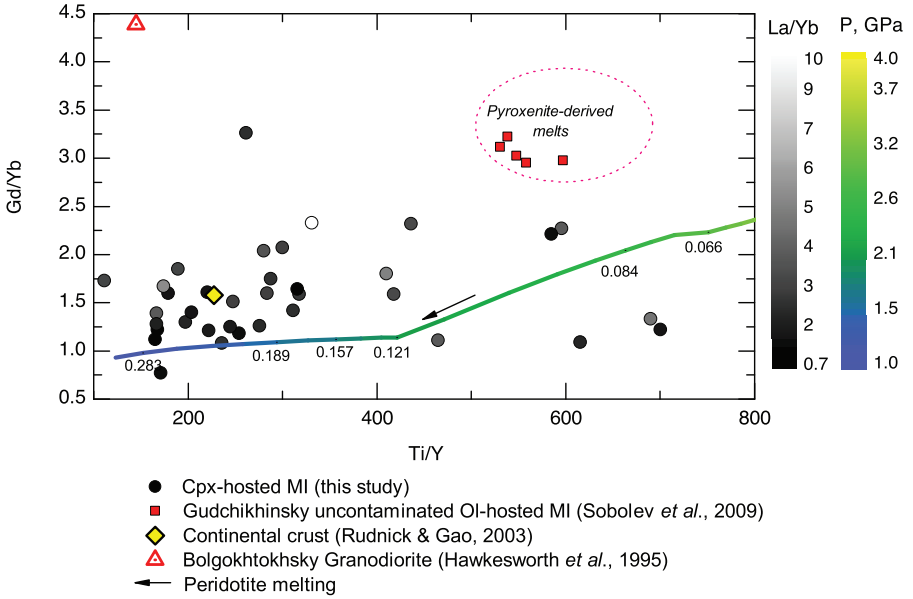

Fig. 10. Gd/Yb vs Ti/Y for analysed cpx-hosted melt inclusions (MI) colour-coded for La/Yb variations. A model curve showing melting of peridotite is colour-coded for pressure, varying from 4 to 1 GPa. Melt fractions are indicated. Shown for comparison are the average composition of continental crust and the Bolgokhtokhsky granodiorite.

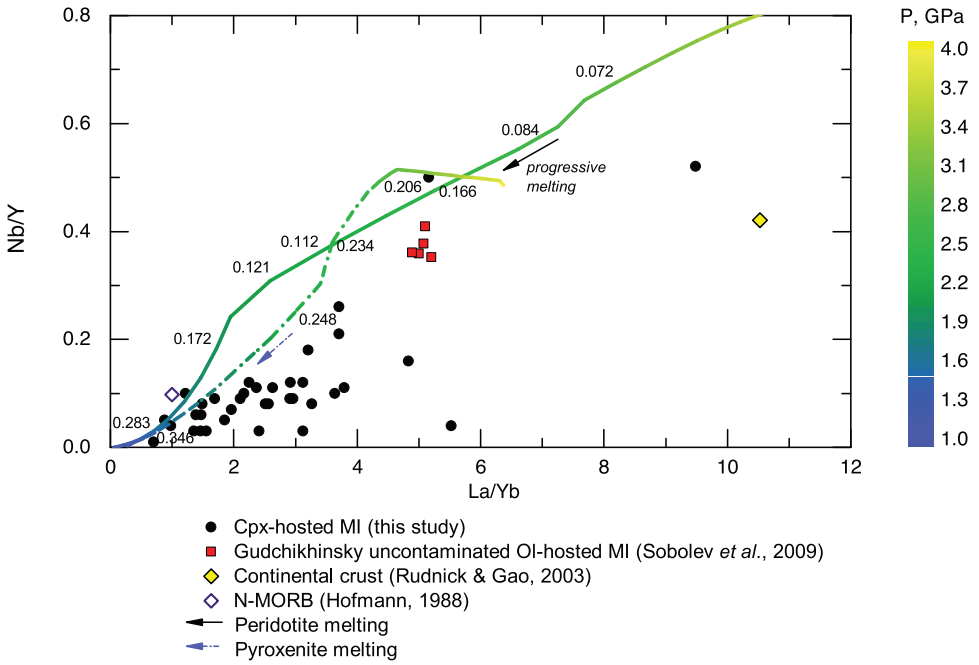

Fig. 11. The variation of Nb/Y vs La/Yb in the analysed cpx-hosted SLIP melt inclusions (MI) from this study compared with MI from the Gudchikhinsky Formation (Sobolev *et al.*, 2009), average continental crust (Rudnick & Gao, 2003) and average N-MORB (Hofmann, 1988). Model curves showing partial melting of peridotite (continuous line) and pyroxenite (short dash–dot line) are colour-coded for pressure, varying from 4 to 1 GPa.

both the latest Permian and earliest Triassic mass extinctions occurred after the emplacement of magmas derived largely from a pyroxenite mantle source. The volatile output of these early high-Ti magmas (Fig. 2) was much greater than that of the meimechites and alkaline magmas erupted later in the sequence, which became volatile-rich owing to their emplacement in evaporites (Fig. 14). The low-Ti basaltic magmas that make up most of the SLIP were derived from a depleted peridotite mantle source and emitted considerably smaller mass burdens of gases. Thus mantle source heterogeneity created a sequence of volcanism that began with immense emissions of climate-altering gases into the atmosphere (associated with melting of a pyroxenite source component) and, with time, gradually evolved into eruptions of more depleted melts with a much lower volatile output. Mapping of mantle composition directly onto atmospheric volatile fluxes during volcanism has been suggested recently for modern-day eruptions (e.g. Iceland, Kilauea) and may be highly significant for our understanding of the environmental impact of long periods of intense volcanism in the geological past.

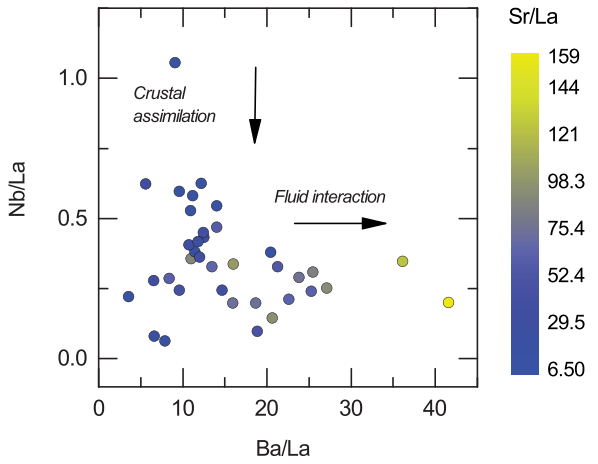

Fig. 12. Nb/La vs Ba/La, colour-coded according to Sr/La. Variability of large ion lithophile and volatile elements is subtracted from fractionation by dividing Nb, Ba and Sr by La.

CONCLUSIONS

The present study was designed to determine the effect of intrinsic mantle source heterogeneity on the

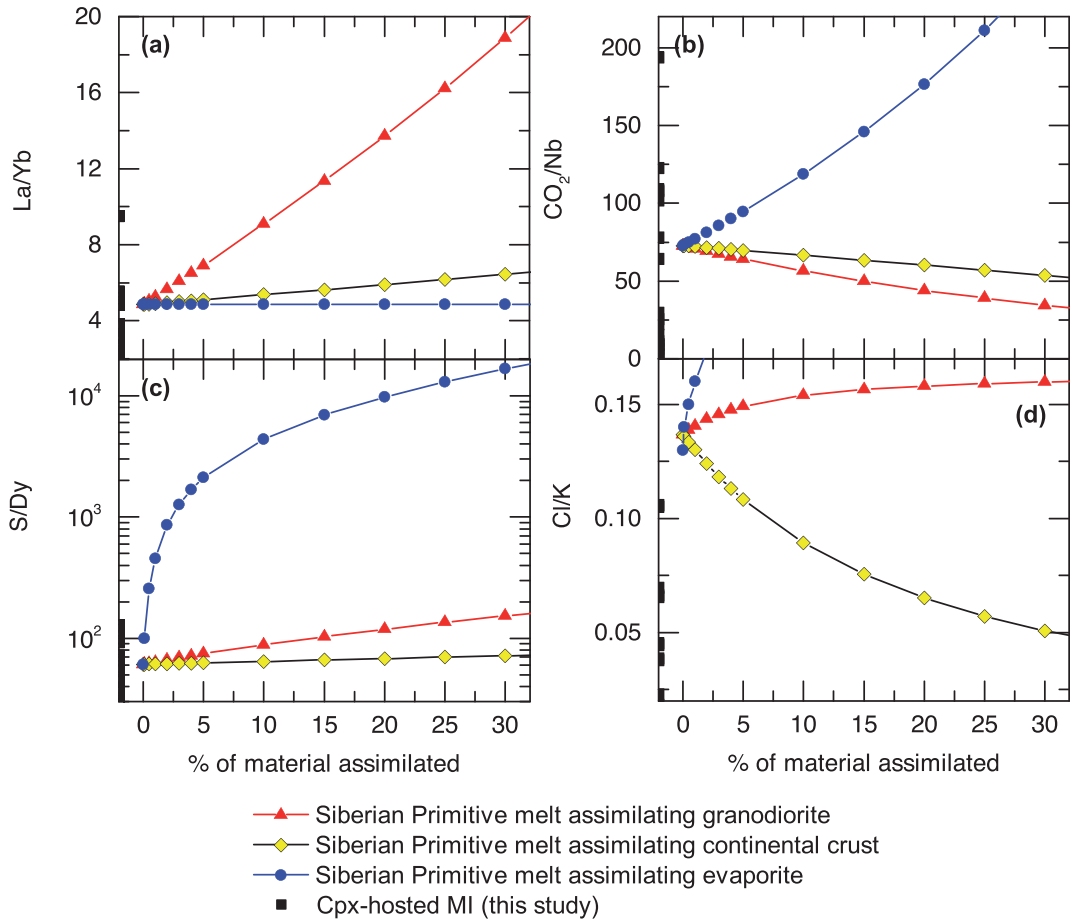

Fig. 13. Changes in elemental ratios with assimilation of different crustal components by the reconstructed primitive Siberian Traps melt composition of Sobolev *et al.* (2009). Ranges of analysed clinopyroxene-hosted melt inclusions from this study are also shown. Data sources: Bolgokhtokhsky granodiorite, Hawkesworth *et al.* (1995); average continental crust, Rudnick & Gao (2003); Devonian sulphate-rich evaporite, Pang *et al.* (2013).

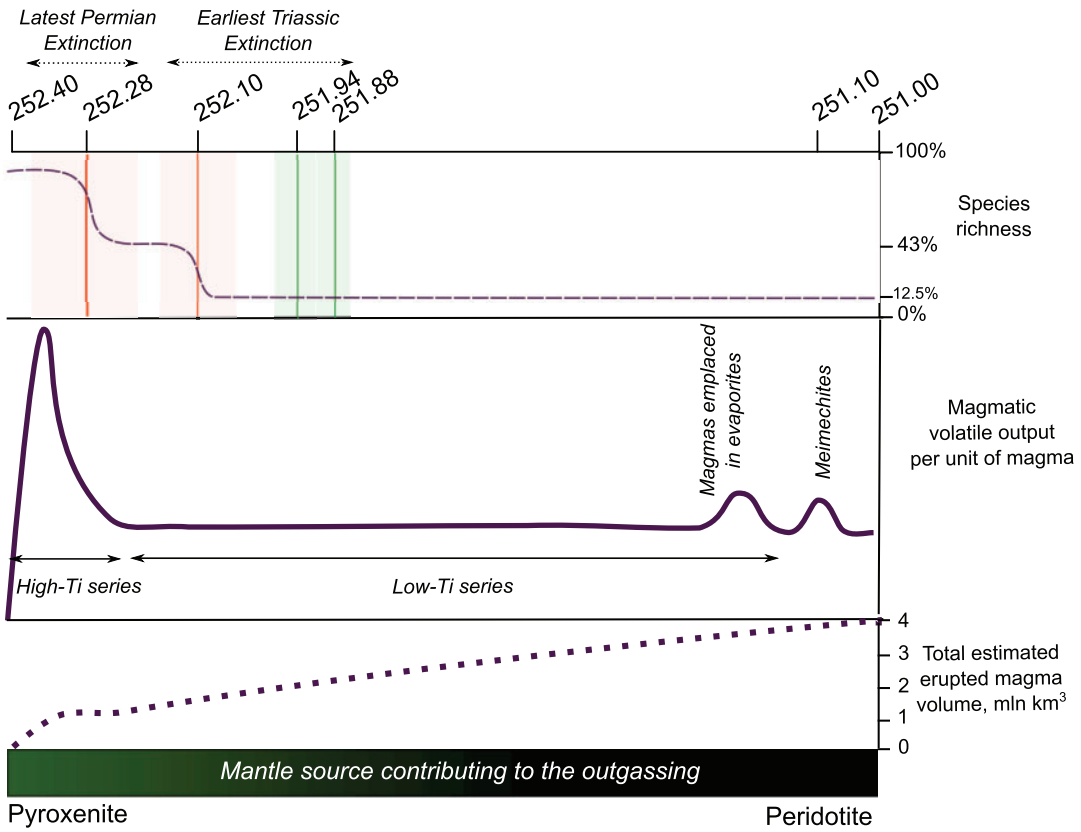

Fig. 14. Magmatic contribution to the total volatile output and mantle source evolution over time. The ages of the mass extinctions are from Song *et al.* (2012) (orange vertical lines with pale orange shaded field representing error bars) and Burgess *et al.* (2014) (green lines and pale green shaded fields). Ages for the onset and the end of magmatic activity are from Kamo *et al.* (2003) and for meimechite emplacement from Arndt *et al.* (1998). High-Ti series magmas make up less than 1 million km^3, which is less than a quarter of the total magma volume. The onsets of both the latest Permian and the earliest Triassic mass extinctions occur after the emplacement of high-Ti pyroxenite-derived chlorine- and carbon-rich magmas. Two-thirds of SLIP magma volume were emplaced before or during the extinction (Burgess & Bowring, 2015).

compositions of SLIP magmas and their volatile outputs. It has been shown that sills and lava flows erupted to the SE of Norilsk were formed from melts that were subject to differentiation, a small amount of crustal contamination, interaction with crustal fluids and degassing (of carbon and sulfur species). Despite all of these superimposed processes, evidence for the mixing of melts derived from differing degrees of melting of a heterogeneous mantle source is preserved. Moreover, this is the second most important parameter controlling the compositional variability of the melts after fractional crystallization. Mixing of melts derived from variable degrees of melting of peridotite containing a small amount of halogen-rich pyroxenite can account for most of the geochemical features observed in the melt inclusion dataset. Overall, the melts are more volatile-poor than those reported from the Gudchikhinsky Formation by Sobolev *et al.* (2009) and from the Bratsk and Ust-Ilimsk sills by Black *et al.* (2012). In the former case it is the result of both an increased proportion of peridotite in the source and a significant amount of dilution by assimilation of volatile-poor continental crust, whereas in the latter it is due to a lack of contamination by evaporites. We suggest that these volatile-poor magmas may have been widespread across the Siberian Craton and that the overall volatile budget of the Siberian Traps Large Igneous Province may have been previously overestimated. More accurate estimates of the magmatic contribution to the total volatile budget require careful asessment of the overall volumes of volatile-rich melts, including those sourced from pyroxenite and those emplaced into volatile-rich sediments.

ACKNOWLEDGEMENTS

The authors thank the NERC Edinburgh Ion Probe facility and Richard Hinton in particular for providing us with the opportunity to perform SIMS analysis. We also acknowledge Iris Buisman for her assistance with EPMA. We also thank Alexander G. Polozov, Sverre Planke, Dougal Jerram and Seth Burgess for their companionship and assistance during field sampling. The paper was considerably improved following helpful reviews by David Peate, Yi-Giang Xu and Andrew Saunders. The authors also thank the editor Marjorie Wilson for careful editing and useful suggestions.

FUNDING

This work was supported by a Natural Environment Research Council (NE/H012648/1) and a Natural Environment Research Council Ion Microprobe Facility award. S.S. acknowledges Trinity Hall (Cambridge, UK) for providing a Mann Studentship towards her PhD studies. The Centre for Physics of Geological Processes, University of Oslo, provided the fieldwork funding.

SUPPLEMENTARY DATA

Supplementary data for this paper are available at *Journal of Petrology* online.

REFERENCES

Aarnes, I., Svensen, H., Connolly, J. A. D. & Podladchikov, Y. Y. (2010). How contact metamorphism can trigger global climate changes: Modeling gas generation around igneous sills in sedimentary basins. *Geochimica et Cosmochimica Acta* **74**, 7179–7195.

Aarnes, I., Svensen, H., Polteau, S. & Planke, S. (2011). Contact metamorphic devolatilization of shales in the Karoo Basin, South Africa, and the effects of multiple sill intrusions. *Chemical Geology* **281**, 181–194.

Anderson, D. L. (1994). The sublithospheric mantle as the source of continental flood basalts; the case against lithosphere and plume head reservoirs. *Earth and Planetary Science Letters* **123**, 269–280.

Arndt, N., Lehnert, K. & Vasiliev, Y. (1995). Maimechites: highly magnesian lithosphere-contaminated alkaline magmas from deep subcontinental mantle. *Lithos* **34**, 41–59.

Arndt, N., Chauvel, C., Czamanske, G. & Fedorenko, V. (1998). Two mantle sources, two plumbing systems: tholeiitic and alkaline magmatism of the Maymecha River basin, Siberian flood province. *Contributions to Mineralogy and Petrology* **133**, 297–313.

Baker, D. R. & Balcone-Boissard, H. (2009). Halogen diffusion in magmatic systems: Our current state of knowledge. *Chemical Geology* **263**, 82–88.

Baker, D. R., Freda, C., Brooker, R. A. & Scarlato, P. (2005). Volatile diffusion in silicate melts and its effects on melt inclusions. *Annals of Geophysics* **48**, 699–717.

Baker, J. A., Thirlwall, M. F. & Menzies, M. A. (1996). Sr–Nd–Pb isotopic and trace element evidence for crustal contamination of plume-derived flood basalts: Oligocene flood volcanism in western Yemen. *Geochimica et Cosmochimica Acta* **60**, 2559–2581.

Balcone-Boissard, H., Baker, D. R., Villemant, B. & Boudon, G. (2009). F and Cl diffusion in phonolitic melts: Influence of the Na/K ratio. *Chemical Geology* **263**, 89–98.

Basu, A. R., Poreda, R. J., Renne, P. R., Teichmann, F., Vasiliev, Y. R., Nikolai, V., Sobolev, N. V & Turrin, B. D. (1995). High-3He plume origin and temporal-spatial evolution of the Siberian flood basalts. *Science* **269**, 822–825.

Baud, A., Magaritz, M. & Holser, W. (1989). Permian–Triassic of Tethys: Carbon isotope studies. *Geologische Rundschau* **78**, 649–677.

Black, B. A., Elkins-Tanton, L. T., Rowe, M. C. & Peate, I. U. (2012). Magnitude and consequences of volatile release from the Siberian Traps. *Earth and Planetary Science Letters* **317–318**, 363–373.

Black, B. A., Hauri, E. H., Elkins-Tanton, L. T. & Brown, S. M. (2014). Sulfur isotopic evidence for sources of volatiles in Siberian Traps magmas. *Earth and Planetary Science Letters* **394**, 58–69.

Brandon, A. D., Hooper, P. R., Gole, G. G. & Lambert, R. J. (1993). Evaluating crustal contamination in continental basalts: the isotopic composition of the Picture Gorge Basalt of the Columbia River Basalt Group. *Contributions to Mineralogy and Petrology* **114**, 452–464.

Brasier, M. D., Shields, G., Kuleshov, V. N. & Zhegallo, E. A. (1996). Integrated chemo- and biostratigraphic calibration of early animal evolution: Neoproterozoic–early Cambrian of southwest Mongolia. *Geological Magazine* **133**, 459–485.

Burgess, S. D. & Bowring, S. (2015). High-precision geochronology confirms voluminous magmatism before, during, and after Earth's most severe extinction. *Science Advances* **1**: e1500470.

Burgess, S. D., Bowring, S. & Shen, S.-Z. (2014). High-precision timeline for Earth's most severe extinction. *Proceedings of the National Academy of Sciences of the USA* **111**(**9**), 3316–3321.

Cabral, R. A., Jackson, M. G., Rose-Koga, E. F., Koga, K. T., Whitehouse, M. J., Antonelli, M. A., Farquhar, J., Day, J. M. D. & Hauri, E. H. (2013). Anomalous sulphur isotopes in plume lavas reveal deep mantle storage of Archaean crust. *Nature* **496**, 490–493.

Campbell, I. H., Czamanske, G. K., Fedorenko, V. A., Hill, R. & Stepanov, V. (1992). Synchronism of the Siberian Traps and the Permian–Triassic boundary. *Science* **258**, 1760–1763.

Courtillot, V., Jaupart, C., Manighetti, I., Tapponnier, P. & Besse, J. (1999). On causal links between flood basalts and continental breakup. *Earth and Planetary Science Letters* **166**, 177–195.

Czamanske, G. K., Gurevitch, A. B., Fedorenko, V. & Simonov, O. (1998). Demise of the Siberian plume: paleogeographic and paleotectonic reconstruction from the prevolcanic and volcanic record, NorthCentral Siberia. *International Geology Reviews* **1**:40, 95–115.

Dalou, C., Koga, K. T., Le Voyer, M. & Shimizu, N. (2014). Contrasting partition behavior of F and Cl during hydrous mantle melting: implications for Cl/F signature in arc magmas. *Progress in Earth and Planetary Science* **1**:26.

Danyushevsky, L. V. (2004). Melt inclusions in primitive olivine phenocrysts: the role of localized reaction processes in the origin of anomalous compositions. *Journal of Petrology* **45**, 2531–2553.

Danyushevsky, L. V., Della-Pasqua, F. N. & Sokolov, S. (2000). Reequilibration of melt inclusions trapped by magnesian olivine phenocrysts from subduction-related magmas: petrological implications. *Contributions to Mineralogy and Petrology* **138**, 68–83.

Danyushevsky, L. V., McNeill, A. W. & Sobolev, A. V. (2002). Experimental and petrological studies of melt inclusions in phenocrysts from mantle-derived magmas: an overview of technique, advantages and complication. *Chemical Geology* **183**, 5–24.

Devey, C. W. & Cox, K. G. (1987). Relationship between crustal contamination and crystallization in continental flood basalt magmas with special reference to the Deccan Traps of the Western Ghats, India. *Earth and Planetary Science Letters* **84**, 59–68.

Elkins-Tanton, L. T. & Hager, B. H. (2000). Melt intrusion as a trigger for lithospheric foundering and the eruption of the Siberian flood basalts. *Geophysical Research Letters* **27**, 3937–3940.

Erwin, D. H. (1990). The end-Permian mass extinction. *Annual Review of Ecology and Systematics* **21**, 69–91.

Ewart, A., Milner, S. C., Armstrong, R. A. & Duncan, A. R. (1998). Etendeka volcanism of the Goboboseb Mountains and Messum Igneous Complex, Namibia. Part I : Geochemical

evidence of Early Cretaceous Tristan plume melts and the role of crustal contamination in the Parana–Etendeka CFB. *Journal of Petrology* **39**, 191–225.

Fedorenko, V., Czamanske, G., Zen'ko, T., Budahn, J. & Siems, D. (2000). Field and geochemical studies of the melilite-rearing Arydzhangsky suite, and an overall perspective on the Siberian alkaline-ultramafic flood-volcanic rocks. *Internatonal Geology Reviews* **42**, 769–804.

Fedorenko, V. A., Lightfoot, P. C., Naldrett, A. J., Czamanske, G. K., Hawkesworth, C. J., Wooden, J. L. & Ebel, D. S. (1996). Petrogenesis of the flood-basalt sequence at Noril'sk, North Central Siberia. *International Geology Review* **38**, 99–135.

Freda, C., Baker, D. R. & Scarlato, P. (2005). Sulfur diffusion in basaltic melts. *Geochimica et Cosmochimica Acta* **69**, 5061–5069.

Gaetani, G. A., O'Leary, J. A., Shimizu, N., Bucholz, C. E. & Newville, M. (2012). Rapid re-equilibration of H_2O and oxygen fugacity in olivine-hosted melt inclusions. *Geology* **40**, 915–918.

Ganino, C. & Arndt, N. T. (2009). Climate changes caused by degassing of sediments during the emplacement of large igneous provinces. *Geology* **37**, 323–326.

Ghiorso, M. S., Hirschmann, M. M., Reiners, P. W. & Kress, V. C. (2002). The pMELTS: A revision of MELTS for improved calculation of phase relations and major element partitioning related to partial melting of the mantle to 3 GPa. *Geochemistry, Geophysics, Geosystems* **3**, 5.

Grinenko, L. I. (1985). Sources of sulfur of the nickeliferous and barren gabbro–dolerite intrusions of the northwest Siberian platform. *International Geology Review* **27**, 695–708.

Hauri, E., Gaetani, G. A. & Green, T. H. (2006). Xtremely reducing conditions reached during basaltic intrusion in organic-bearing sediments. *Earth and Planetary Science Letters* **248**, 715–734.

Hawkesworth, C. J., Lightfoot, P. C., Fedorenko, V. A., Blake, S., Naldrett, A. J., Doherty, W. & Gorbachev, N. S. (1995). Magma differentiation and mineralisation in the Siberian continental flood basalts. *Lithos* **34**, 61–88.

Heinonen, J. S., Carlson, R. W., Riley, T. R., Luttinen, A. V. & Horan, M. F. (2014). Subduction-modified oceanic crust mixed with a depleted mantle reservoir in the sources of the Karoo continental flood basalts. *Earth and Planetary Science Letters* **394**, 229–241.

Herzberg, C. (2006). Petrology and thermal structure of the Hawaiian plume from Mauna Kea volcano. *Nature* **444**, 605–609.

Hofmann, A. W. (1988). Chemical differentiation of the Earth: the relationship between mantle, continental crust, and oceanic crust. *Earth and Planetary Science Letters* **90**, 297–314.

Hofmann, A. W. & White, M. W. (1982). Mantle plumes from ancient crust. *Earth and Planetary Science Letters* **57**, 421–436.

Iacono-Marziano, G., Gaillard, F., Scaillet, B., Alexander, G. & Arndt, N. T. (2012). Extremely reducing conditions reached during basaltic intrusion in organic-bearing sediments. *Earth and Planetary Science Letters* **357–368**, 308–318.

Isozaki, Y. (1997). Permo-Triassic boundary superanoxia and stratified superocean: records from lost deep sea. *Science* **276**, 235–238.

Ivanov, A. V. & Litasov, K. D. (2014). The deep water cycle and flood basalt volcanism. *International Geology Review* **56**, 1.

Kamenetsky, V. S., Chung, S.-L., Kamenetsky, M. B. & Kuzmin, D. V. (2012). Picrites from the Emeishan Large Igneous Province, SW China: a compositional continuum in primitive magnas and their respective mantle sources. *Journal of Petrology* **53**, 1095–2113.

Kamo, S. L., Czamanske, G. K., Amelin, Y., Fedorenko, V. A., Davis, D. W. & Trofimov, V. R. (2003). Rapid eruption of Siberian flood-volcanic rocks and evidence for coincidence with the Permian–Triassic boundary and mass extinction at 251 Ma. *Earth and Planetary Science Letters* **214**, 75–91.

Kaufman, A. J., Knoll, A. H., Semikhatov, M., Grotzinger, J. P., Jacobsen, S. B. & Adams, W. R. (1996). Isotopic chemostratigraphy of Precambrian–Cambrian boundary beds in the Western Anabar Region, Northern Siberia. *Geological Magazine* **133**, 509–533.

Kendrick, M. A., Jackson, M. G., Kent, A. J. R., Hauri, E. H., Wallace, P. J. & Woodhead, J. (2014). Contrasting behaviours of CO_2, S, H_2O and halogens (F, Cl, Br and I) in enriched-mantle melts from Pitcairn and Society seamounts. *Chemical Geology* **370**, 69–81.

Kent, A. J. R. (2008). Melt inclusions in basaltic and related volcanic rocks. In: Putirka, K. D. & Tepley, F. J., III (eds) *Minerals, Inclusions and Volcanic Processes. Mineralogical Society of America and Geochemical Society, Reviews in Mineralogy and Geochemistry* **69**, 273–331.

Krivoluskaya, N. A. (2001). Magmatic inclusions in olivines from intrusions of the Norilsk's Region, Northwestern Platform: Evidence for Primary melts. *Doklady Earth Sciences* **381A**, 1047–1052.

Krivolutskaya, N. A., Plechova, A. A., Belyatskii, B. V., Roshchina, I. A., Svirskaya, N. M. & Kononkova, N. N. (2014). Geochemical aspects of the assimilation of host rocks by basalts during the formation of Norilsk Cu–Ni ores. *Petrology* **22**, 128–150.

Le Voyer, M., Asimow, P. D., Mosenfelder, J. L., Guan, Y., Wallace, P. J., Schiano, P., Stolper, E. M. & Eiler, J. M. (2014). Zonation of H_2O and F concentrations around melt inclusions in olivines. *Journal of Petrology* **55**, 685–707.

Lightfoot, P. C., Naldrett, A. J., Gorbachev, N. S., Doherty, W. & Fedorenko, V. A. (1990). Geochemistry of the Siberian Trap of the Noril'sk area, USSR, with implications for the relative contributions of the crust and mantle to flood basalt magmatism. *Contributions to Mineralogy and Petrology* **104**, 631–644.

Lightfoot, P. C., Hawkesworth, C. J., Hergt, J., Naldrett, A. J., Gorbachev, N. S., Fedorenko, V. A. & Doherty, W. (1993). Remobilisation of the continental lithosphere by a mantle plume: from picritic and tholeiitic lavas of the Noril'sk District, Siberian Traps, Russia. *Contributions to Mineralogy and Petrology* **114**, 171–188.

Maclennan, J., McKenzie, D., Grönvold, K., Shimizu, N., Eiler, J. M. & Kitchen, N. (2003). Melt mixing and crystallization under Theistareykir, northeast Iceland. *Geochemistry, Geophysics, Geosystems* **4**, 11.

Malich, N. S., Tazihin, N. N., Tuganova, E. V., Bunzen, E. A., Kulikova, N. G. & Safonova, I. V. (1974). *Map of geological formations of the Siberian platform cover (1:1 500 000)*. All-Union Research Geologic Institute (VSEGEI).

Mather, T. A. (2008). Volcanism and the atmosphere: the potential role of the atmosphere in unlocking the reactivity of volcanic emissions. *Philosophical Transactions of the Royal Society of London, Series A* **366**, 4581–4595.

McDonough, W. F. & Sun, S. (1995). The composition of the Earth. *Chemical Geology* **120**, 223–253.

Naldrett, A. J., Lightfoot, P. C., Fedorenko, V., Doherty, W. & Gorbachev, N. S. (1992). Geology and geochemistry of intrusions and flood basalts of the Noril'sk Region, USSR, with implications for the origin of the Ni–Cu ores. *Economic Geology* **87**, 975–1004.

Nielsen, R. L., Crum, J., Bourgeois, R., Hascall, K., Forsythe, L. M., Fisk, M. R. & Christie, D. M. (1995). Melt inclusions in high-An plagioclase from the Gorda Ridge: an example of

the local diversity of MORB parent magmas. *Contributions to Mineralogy and Petrology* **122**, 34–50.

Pang, K.-N., Arndt, N., Svensen, H., Planke, S., Polozov, A., Polteau, S., Iizika, Y. & Ching, S.-L. (2013). A petrologic, geochemical and Sr–Nd isotopic study on contact metamorphism and degassing of Devonian evaporites in the Norilsk aureoles, Siberia. *Contributions to Mineralogy and Petrology* **165**, 683–704.

Petrychenko, O. Y., Peryt, T. M. & Chechel, E. I. (2005). Early Cambrian seawater chemistry from fluid inclusions in halite from Siberian evaporites. *Chemical Geology* **219**, 149–161.

Portnyagin, M., Almeev, R., Matveev, S. & Holtz, F. (2008). Experimental evidence for rapid water exchange between melt inclusions in olivine and host magma. *Earth and Planetary Science Letters* **272**, 541–552.

Putirka, K. D. (2008). Thermometers and barometers for volcanic systems. In: Putirka, K. D. & Tepley, F. J., III (eds) *Minerals, Inclusions and Volcanic Processes. Mineralogical Society of America and Geochemical Society, Reviews in Mineralogy and Geochemistry* **69**, 61–120.

Putirka, K. D., Mikaelian, H., Ryerson, F. & Shaw, H. (2003). New clinopyroxene–liquid thermobarometers for mafic, evolved, and volatile-bearing lava compositions, with applications to lavas from Tiber and the Snake River Plain, Idaho. *American Mineralogist* **88**, 1542–1554.

Reichow, M. K., Saunders, A., White, R., Al'Mukhamedov, A. & Medvedev, A. (2005). Geochemistry and petrogenesis of basalts from the West Siberian Basin: an extension of the Permo-Triassic Siberian Traps, Russia. *Lithos* **79**, 425–452.

Reichow, M. K., Saunders, A. D., White, R. V., Pringle, M. S., Al'Mukhamedov, A. I., Medvedev, A. Ya. & Kirda, N. P. (2002). 40Ar/39Ar dates from the West Siberian Basin: Siberian Flood Basalt Province doubled. *Science* **296**, 1846–1849.

Reichow, M. K., Pringle, M. S., Al'Mukhamedov, A. I., Allen, M. B., Andreichev, V. L., Buslov, M. M., Davies, C. E., Fedoseev, G. S., Fitton, J. G., Inger, S., Medvedev, A., Mitchell, C., Puchkov, V. N., Safonova, I. Y., Scott, R. A. & Saunders, A. D. (2009). The timing and extent of the eruption of the Siberian Traps large igneous province: Implications for the end-Permian environmental crisis. *Earth and Planetary Science Letters* **277**, 9–20.

Renne, P. R. & Basu, A. R. (1991). Rapid eruption of Siberian Traps flood basalts at Permo-Triassic boundary. *Science* **253**, 176–179.

Renne, P. R., Zhang, Z., Richards, M. A., Black, M. T. & Basu, A. R. (1995). Synchrony and causal relations between Permian–Triassic boundary crises and Siberian flood volcanism. *Science* **269**, 1413–1416.

Richards, M. A., Duncan, R. A. & Courtillot, V. E. (1989). Flood basalts and hot-spot tracks: plume heads and tails. *Science* **246**, 103–107.

Ripley, E. M., Park, Y. R., Lambert, D. D. & Frick, L. R. (2001). Re–Os isotopic variations in carbonaceous pelites hosting the Duluth Complex: Implications for metamorphic and metasomatic processes associated with mafic magma chambers. *Geochimica et Cosmochimica Acta* **65**, 2965–2978.

Ripley, E. M., Lightfoot, P. C., Li, C. & Elswick, E. R. (2003). Sulfur isotopic studies of continental flood basalts in the Norilsk region: implications for the association between lavas and ore-bearing intrusions. *Geochimica et Cosmochimica Acta* **67**, 2805–2817.

Rosenthal, A., Hauri, E. H. & Hirschmann, M. M. (2015). Experimental determination of C, F, and H partitioning between mantle minerals and carbonated basalt, CO_2/Ba and CO_2/Nb systematics of partial melting, and the CO_2 contents of basaltic source regions. *Earth and Planetary Science Letters* **412**, 77–87.

Rudge, J. F., Maclennan, J. & Stracke, A. (2013). The geochemical consequences of mixing melts from a heterogeneous mantle. *Geochimica et Cosmochimica Acta* **114**, 112–143.

Rudnick, R. L. & Gao, S. (2003). Composition of the continental crust. In: Rudnick, R. L. (ed.) *The Crust. Treatise on Geochemistry 3*. Elsevier, pp. 1–64.

Saal, A. E., Hauri, E. H., Langmuir, C. H. & Perfit, M. R. (2002). Vapour undersaturation in primitive mid-ocean-ridge basalt and the volatile content of Earth's upper mantle. *Nature* **419**, 451–455.

Saunders, A. D., England, R. W., Reichow, M. K. & White, R. V. (2005). A mantle plume origin for the Siberian traps: uplift and extension in the West Siberian Basin, Russia. *Lithos* **79**, 407–424.

Self, S., Thordarson, T. & Widdowson, M. (2005). Gas fluxes from flood basalt eruptions. *Elements* **1**, 283–287.

Shorttle, O. & Maclennan, J. (2011). Compositional trends of Icelandic basalts: Implications for short-length scale lithological heterogeneity in mantle plumes. *Geochemistry, Geophysics, Geosystems* **12**, 11.

Smith, P. M. & Asimow, P. D. (2005). Adiabat_1ph: A new public front-end to the MELTS, pMELTS, and pHMELTS models. *Geochemistry, Geophysics, Geosystems* **6**, 1, doi:10.1029/2004GC000816.

Sobolev, A. V. & Shimizu, N. (1993). Ultra-depleted primary melt included in an olivine from the Mid-Atlantic ridge. *Nature* **363**, 151–154.

Sobolev, A. V., Hofmann, A. W., Sobolev, S. V. & Nikogosian, I. K. (2005). An olivine-free mantle source of Hawaiian shield basalts. *Nature* **434**, 590–597.

Sobolev, A. V., Hofmann, A. W., Kuzmin, D. V., et al. (2007). The amount of recycled crust in sources of mantle-derived melts. *Science* **316**, 412–417.

Sobolev, A. V., Krivolutskaya, N. A. & Kuzmin, D. V. (2009). Petrology of the parental melts and mantle sources of Siberian trap magmatism. *Petrology* **17**, 253–286.

Sobolev, S. V., Sobolev, A. V., Kuzmin, D. V., Krivolutskaya, N. A., Petrunin, A. G., Arndt, N. T., Radko, V. A. & Vasiliev, Y. R. (2011). Linking mantle plumes, large igneous provinces and environmental catastrophes. *Nature* **477**, 312–316.

Sobolev, A. V., Arndt, N. T., Krivolutskaya, N. A., Kuzmin, D. Y. & Sobolev, S. V. (2015). The origin of gases that caused Permo-Triassic extinction. In: Schmidt, A., Fristad, K. E. & Elkins-Tanton, L. T. (eds) *Volcanism and Global Environmental change*. Cambridge University Press, pp. 147–163.

Song, H., Wignall, P. B., Tong, J. & Yin, H. (2012). Two pulses of extinction during the Permian–Triassic crisis. *Nature Geoscience* **6**, 52–56.

Stracke, A., Zindler, A., Salters, V. J. M., McKenzie, D., Blichert-Toft, J., Albarède, F. & Grönvold, K. (2003). Theistareykir revisited. *Geochemistry, Geophysics, Geosystems* **4**, 8507.

Sun, S. & McDonough, W. F. (1989). Chemical and isotopic systematics of oceanic basalts: implications for mantle composition and processes. In: Saunders, A. D. & Norry, M. J. (eds) *Magmatism in the Ocean Basins. Geological Society, London, Special Publications* **42**, 313–345.

Svensen, H., Planke, S., Polozov, A. G., Schmidbauer, N., Corfu, F., Podladchikov, Y. Y. & Jamtveit, B. (2009). Siberian gas venting and the end-Permian environmental crisis. *Earth and Planetary Science Letters* **277**, 490–500.

Tait, S. (1992). Selective preservation of melt inclusions in igneous phenocrysts. *American Mineralogist* **77**, 146–155.

Takahashi, E. (1986). Melting of dry peridotite KLB-1 up to 14 GPa: implications on the origin of peridotitic upper mantle. *Journal of Geophysical Research* **91**, 9367–9382.

Tang, Q., Zhang, M., Li, C., Yu, M. & Li, L. (2013). The chemical compositions and abundances of volatiles in the Siberian large igneous province: Constraints on magmatic CO_2 and SO_2 emissions into the atmosphere. *Chemical Geology* **339**, 84–91.

Vasiliev, Y. R., Zolotukhin, V. V., Feoktistov, G. D. & Prusskaya, S. N. (2000). Evaluation of the volume and genesis of Permo-Triassic Trap magmatism on the Siberian Platform. *Russian Geology and Geophysics* **41**, 1696–1705.

White, R. V. (2002). Earth's biggest 'whodunnit': unravelling the clues in the case of end-Permian mass extinction. *Philosophical Transactions of the Royal Society of London, Series A* **360**, 2963–2985.

White, R. V. & Saunders, A. D. (2005). Volcanism, impact and mass extinctions: incredible or credible coincidences? *Lithos* **79**, 299–316.

Wignall, P. B. (2001). Large igneous provinces and mass extinctions. *Earth-Science Reviews* **53**, 1–33.

Wooden, J. L., Czamanske, G. K., Fedorenko, V. A., Arndt, N. T., Chauvel, C., Bouse, R. M., King, B.-S. W., Knight, R. J. & Siems, D. F. (1993). Isotopic and trace-element constraints on mantle and crustal contributions to Siberian continental flood basalts, Noril'sk area, Siberia. *Geochimica et Cosmochimica Acta* **57**, 3677–3704.

Workman, R. K. & Hart, S. R. (2005). Major and trace element composition of the depleted MORB mantle (DMM). *Earth and Planetary Science Letters* **231**, 53–72.

Workman, R. K., Hauri, E., Hart, S. R., Wang, J. & Blusztajn, J. (2006). Volatile and trace elements in basaltic glasses from Samoa: Implications for water distribution in the mantle. *Earth and Planetary Science Letters* **241**, 932–951.

Xu, Y. G., Chung, S. L., Jahn, B. M. & Wu, G. Y. (2001). Petrologic and geochemical constraints on the petrogenesis of Permian–Triassic Emeishan flood basalts in southwestern China. *Lithos* **58**, 145–168.

Zharkov, M. A. (1984). *Paleozoic Salt Bearing Formations of the World*. Springer.

Zolotukhin, V. V. & Al'Mukhamedov, A. I. (1988). Traps of the Siberian platform. In: Macdougall, J. D. (eds) *Continental Flood Basalts*. Kluwer Academic, pp. 273–310.